ACADÉMIE
DES SCIENCES
INSTITUT DE FRANCE

Comptes Rendus

Géoscience

Sciences de la Planète

Olivier Fabbri, Hugues Raimbourg and Henri Leclère

Fluids, faulting and earthquakes in the brittle crust: recent advances and new challenges

Volume 356, Special Issue S2 (2024), p. 423-466

Online since: 21 May 2024

Part of Special Issue: Geodynamics of Continents and Oceans – A tribute to Jean Aubouin

Guest editors: Olivier Fabbri (Université de Franche-Comté, UMR CNRS 6249, Besançon), Michel Faure (Université d'Orléans-BRGM, UMR CNRS 7325, Institut des Sciences de la Terre, Orléans), Jacky Ferrière (Université de Lille, faculté des Sciences), Laurent Jolivet (Sorbonne Université, ISTeP, UMR 7193, Paris) and Sylvie Leroy (Sorbonne Université, CNRS-INSU, ISTeP, Paris)

https://doi.org/10.5802/crgeos.259

CENTRE MERSENNE

The Comptes Rendus. Géoscience — Sciences de la Planète *are a member of the Mersenne Center for open scientific publishing*
www.centre-mersenne.org — e-ISSN : 1778-7025

ACADÉMIE DES SCIENCES
INSTITUT DE FRANCE

Comptes Rendus. Géoscience — Sciences de la Planète
2024, Vol. 356, Special issue S2, p. 423-466
https://doi.org/10.5802/crgeos.259

Research article

Geodynamics of Continents and Oceans – A tribute to Jean Aubouin

Fluids, faulting and earthquakes in the brittle crust: recent advances and new challenges

Olivier Fabbri [*, a], **Hugues Raimbourg** [b] and **Henri Leclère** [a]

[a] UMR 6249, université de Franche-Comté, 16 route de Gray, 25030 Besançon cedex, France

[b] UMR 7327, universite d'Orléans, 1A rue de la Férollerie, 45071 Orléans cedex 2, France

E-mail: olivier.fabbri@univ-fcomte.fr (O. Fabbri)

Abstract. Interactions between fluids and deformation are widespread in the brittle crust. As experimentally shown, a high pore fluid pressure p_f can fracture intact rocks or reactivate pre-existing fractures. The preference of reactivation over the formation of a new fracture depends on the orientation of the pre-existing fracture with respect to the stress axes and on p_f. In nature, the predominant reactivation of misoriented pre-existing faults rather than the formation of new faults with more favorable orientations suggests that pressurized fluids are present in the brittle crust. There is a large body of evidence indicating that supra-hydrostatic p_f contributes to the reactivation of low-angle thrust faults or normal faults. Conversely, supra-hydrostatic p_f values are less common along vertical or steeply dipping plate boundary transform faults or intra-continental strike-slip faults. If these faults are severely misoriented with respect to the ambient stress field, their reactivation may not be due to supra-hydrostatic p_f but to other mechanisms such as shear-enhanced compaction or thermal pressurization. Supra-hydrostatic p_f also plays a role in the nucleation or propagation of seismic ruptures in the continental or oceanic crust, and in subducting slabs in convergent margins, as reported for aftershocks, swarms, slow earthquakes, and to a lesser extent for major earthquakes. Lastly, increase or decrease of p_f in depth due to human activities such as hydrocarbon extraction, dam impoundment, gas storage or geothermal energy production result in many cases in the inception or enhancement of seismic activiy, adding clues in favor of a relationship between fluids and earthquakes.

Keywords. Fluid, Fault, Pore fluid pressure, Earthquake, Slow earthquake, Seismic swarm, Crack-seal vein.

Manuscript received 8 December 2023, revised 12 April 2024, accepted 15 April 2024.

1. Introduction

Whatever their nature, chemical composition or physical state, fluids play key roles in the evolution of the Earth's lithosphere, particularly regarding sediment diagenesis, volcanic activity, hydrothermal alteration, metamorphism, ore deposit formation, among many other phenomena. Fluids are also important with regard to deformation, especially brittle deformation. In the upper brittle crust, fluids can circulate in deforming zones, namely fracture zones or fault zones, and can chemically or mechanically interact with host rocks. Such interactions are also conceivable in subduction zones, where the upper part of the subducting plate keeps a brittle behavior down to hundreds of kms of depth.

* Corresponding author

The role that fluids exert on rock deformation is of paramount importance for human societies. Indeed, fluid extraction (e.g., hydrocarbon industry) or fluid injection (geothermal energy, waste water disposal, gas storage) trigger or enhance seismic activities in otherwise aseismic or moderately active regions.

This review aims at bridging the gap between the mechanical interactions between fluids and rocks on one hand and the structural analysis of deformed rocks from the scale of the hand sample to that of the deforming plate boundaries. For space reasons, the chemical effects of fluids, although of considerable importance, will not be addressed here.

2. The mechanical interaction between fluids and rocks

2.1. *The development of abnormally high pore fluid pressures in the upper crust*

Production of fluid in depth, for instance by magmatic activity or by metamorphic or metasomatic reactions, can result in an influx of fluids. If there is a permeability barrier that prevents or hinders fluid escape, then the pore fluid pressure p_f will increase. This increase can also be generated by pore volume reduction in low-permeability rocks. For instance, elastic crack relaxation following an earthquake (seismic pumping, see below Section 2.6) or inelastic pore compaction controlled by the applied shear stress (shear-enhanced compaction, see below Section 2.7) are two important mechanisms responsible for pore volume decrease. Beside such earthquake-related mechanisms, pore compaction can also be achieved during diagenesis [Walder and Nur, 1984, Wang et al., 2022]. As attested by measurements in deep boreholes, supra-hydrostatic p_f values actually develop below impermeable barriers or seals, and can reach the value of the lithostatic stress or even exceed it [Yerkes et al., 1985, Powley, 1990, Neuzil, 1995, Zencher et al., 2006].

2.2. *Intact rock fracturing, stress corrosion, hydrofracturing*

Classical rupture criteria for *intact rocks* in the upper crust are inspired by experimental rock mechanics and state that, as long as the stress tensor (whose components are σ_1, σ_2, and σ_3, with the convention $\sigma_1 > \sigma_2 > \sigma_3$) acting on the rock does not satisfy any criterion, no fracture will form. To the contrary, once the stress tensor satisfies the criterion, microscopic fractures will propagate through the rock, eventually leading to the formation of a macroscopic fracture or fault.

Two rupture criteria are commonly used in the analysis of intact rock failure. The simplest is the linear Mohr–Coulomb criterion, which postules that the propagation of macroscopic fractures happens when

$$\tau = \mu_i \sigma_n + C$$

with τ being the tangential stress acting along the fracture, σ_n the normal stress acting on the fracture, μ_i and C being respectively the intrinsic coefficient of friction and the intrinsic cohesion, both depending on rock type. The more elaborated parabolic Griffith failure criterion can be expressed as

$$\tau^2 + 4T\sigma_n = 4T^2$$

where T is the tensile strength of the intact rock, counted positive. Both Mohr–Coulomb and Griffith criteria can be combined in a composite criterion for which the parabolic criterion will apply to negative normal stress values and the linear criterion will apply for the positive normal stress values [Sibson and Scott, 1998; Figure 1].

In the absence of pore fluid in the rock, the convergence between the tensor and the criterion can be achieved only by increasing the differential (deviatoric) stress $\sigma_D = \sigma_1 - \sigma_3$, that is, either by decreasing σ_3, by increasing σ_1, or by acting on both σ_3 and σ_1. If a fluid is present inside the rock (so-called pore fluid), then two processes can lead to the formation of macroscopic fractures. In the first process, called stress corrosion, the fluid will *chemically* react at the atomic scale with the rock at the tip of a pre-existing loaded crack, so that the critical stress intensity factor at this location gets lower and lower. When the stress intensity factor at the tip of the crack reaches the fracture toughness of the altered rock, the fracture will propagate. This phenomenon is called sub-critical crack growth [Anderson and Grew, 1977, Atkinson, 1984, Brantut et al., 2013]. The second process requires that the pore fluid is elevated at a pressure p_f. If so, the components σ_i of the tensor will then be changed into *effective* components $\sigma_i^* = \sigma_i - p_f$, and the rupture criterion is assessed using effective stress.

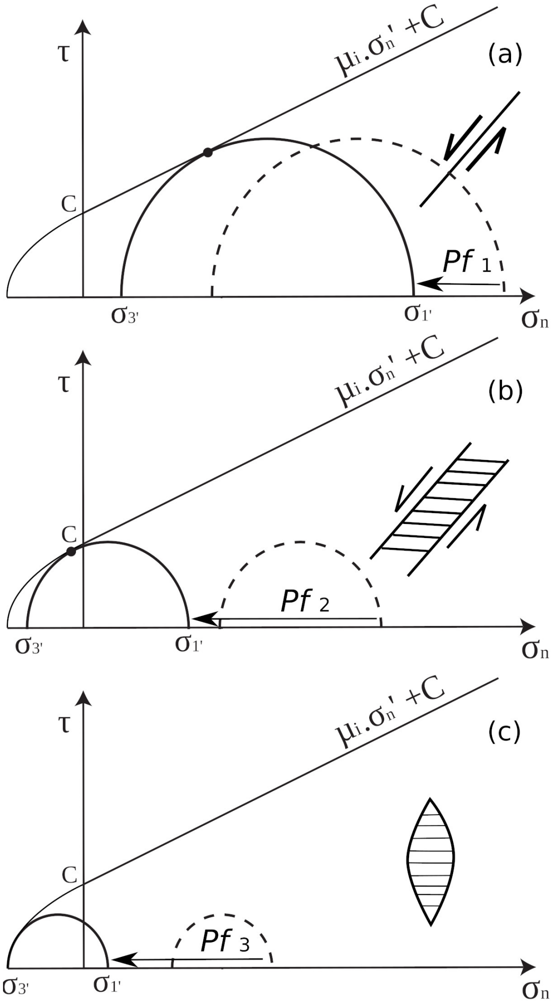

Figure 1. The role of pore fluid pressure in fracturing intact rocks as representated in the Mohr space. The intact rock rupture criterion is composite, that is, it consists of the Griffith criterion for the negative normal stresses, and of the linear Mohr–Coulomb criterion for the positive normal stresses. σ'_n: effective normal stress acting on the surface ($\sigma'_n = \sigma_n - p_f$). (a) A pore fluid pressure p_{f1} decreases the normal stresses and shifts the Mohr circle until it tangents the failure envelope. The orientation of the newly formed fracture with respect to the stress axes is optimal. (b) Due to a lower differential stress, a pore fluid pressure p_{f2} displaces the Mohr circle until it tangents the failure envelope in the parabolic part, resulting in the formation of hybrid shear-extensional fractures.

Figure 1. (**cont.**) (c) Due to a still lower differential stress, a pore fluid pressure p_{f3} displaces the Mohr circle until it tangents the failure envelope at $\tau = 0$, resulting in the formation of pure dilatant fractures.

If p_f is increased enough, the effective stress tensor will satisfy the rupture criteron (Figures 1 and 2). Note that, unlike the σ_i components of the tensor, σ_D is not modified by any variation of p_f. A failure mode diagram [Cox, 2010] allows to estimate σ_D and p_f required for rock failure (Figure 3). In this diagram, p_f is expressed by the pore fluid factor (also called pore fluid pressure ratio) $\lambda = p_f/\rho g z$, where $\rho g z$ is the lithostatic stress, ρ the mean density of the rock column from the surface to depth z, and g the gravity acceleration. The values of λ are between 0.3–0.4 (hydrostatic p_f) and 1 (lithostatic p_f). In a Mohr–Coulomb diagram, if the tangent point between the Mohr circle and the envelope is located in positive σ_n values, the rupture is said to be of shear failure type. This is illustrated in the failure mode diagram by the blue line on the failure envelope (Figures 1a and 3). If $\sigma_3^* = -T$, T being the tensile strength of the intact rock, counted positive, the rupture is purely extensional (dilatant), and is illustrated in the failure mode diagram by the red line on the failure envelope (Figures 1c and 3). It is important to note that the use of extension here does not reflect an extensional tectonic regime (for which $\sigma_V = \sigma_1$, σ_V being the principal vertical stress component, in an Andersonian framework). Intermediate locations correspond to hybrid extensional-shear failures illustrated in the failure mode diagram by the green line on the failure envelope (Figures 1b and 3).

Dilatant breccias form when the three effective principal stresses are negative ($\sigma_3^* < \sigma_2^* < \sigma_1^* < 0$), while *pure* dilatant breccias, that is, breccias without any preferred orientation of dilatancy (Figure 4), form when the stress tensor is hydrostatic, the common stress magnitude being the opposite of the tensile strength of the rock: $\sigma_1^* = \sigma_2^* = \sigma_3^* = -T$ [hydrostatic stress state; Cosgrove, 1995].

Mineralized extensional joints (tension gashes) are typical and widespread geological structures resulting from failure of intact rocks by pure extension (Figure 1c). Pure extension is achieved by the condition $\sigma_3^* = -T$, that is, $p_f = \sigma_3 + T$ [Hubbert and Willis, 1957, Secor, 1965, Hancock, 1985]. The

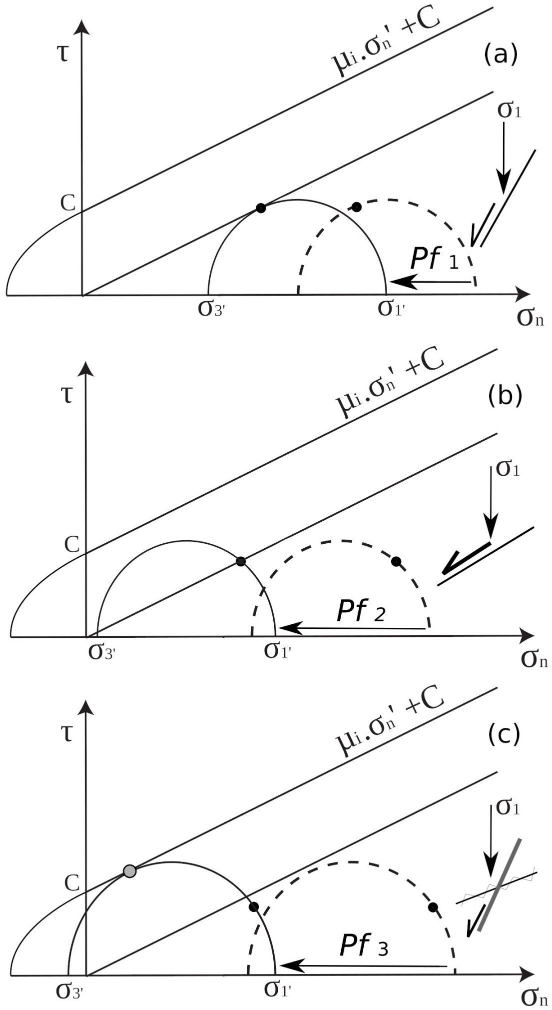

Figure 2. Competition between reactivation of pre-existing fractures and formation of a new fracture [after Handin, 1969, Sibson, 1985]. The failure envelope for intact rock follows a composite Griffith–Mohr–Coulomb criterion. The reactivation envelope is linear, and its cohesion is neglected. σ'_n: effective normal stress acting on the surface ($\sigma'_n = \sigma_n - p_f$). (a) The pre-existing fracture (black dot on the circle) is *favorably oriented* with respect to the σ_1 stress axis. The pore fluid pressure p_{f1} is large enough to allow its reactivation. (b) The pre-existing fracture is *unfavorably oriented* with respect to the σ_1 stress axis, but the *misorientation is moderate*. The pore fluid pressure p_{f2}, larger than p_{f1}, is necessary to allow its reactivation. (c) The pre-existing fracture is *unfavorably oriented* with respect to the σ_1 stress axis, and the *misorientation is severe*.

Figure 2. (**cont**.) Due to an increasing pore fluid pressure, the Mohr circle shifts towards smaller normal stresses. It eventually tangents the intact rock failure envelope (grey dot) before the pre-existing fracture (black dot) can be reactivated. In this case, a new fracture (grey dot) with a favorable orientation is formed for a pore fluid pressure p_{f3}.

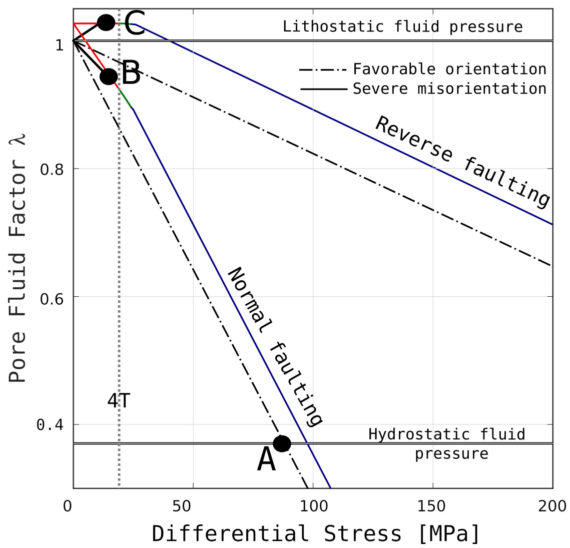

Figure 3. Failure mode diagram for reverse and normal faulting based on the Mohr–Coulomb theory. Red, green and blue lines correspond respectively to pure extensional (dilatant) veins, hybrid veins and shear fractures. Oblique black lines correspond to the reactivation conditions for a favorably oriented fracture or a severely misoriented fracture. The diagram is drawn for a depth z of 7 km, a rock density ρ of 2.7, a friction coefficient μ of 0.75 and a tensile strength T of 5 MPa. See text for explanation of points A, B and C.

regular and symmetrical layering of the minerals filling extension joints suggests a cyclical process with incremental opening stages alternating through time with fluid ingression and crystallization [Ramsay, 1980]. This so-called crack-seal mechanism, reminiscent of the cyclical nature of earthquakes, is often considered as a geological expression of the seismic cycle [see below and Raimbourg et al., 2021, 2022].

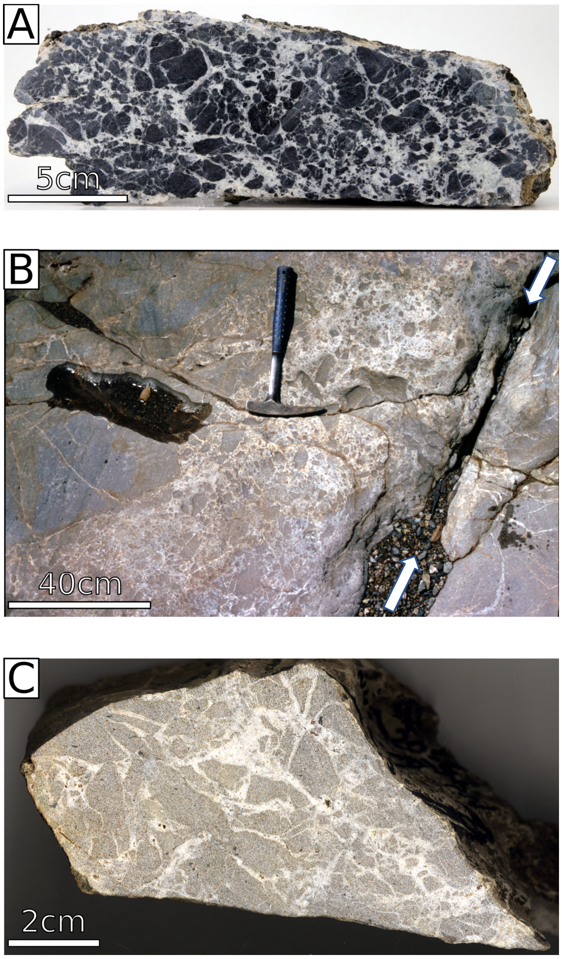

Figure 4. Purely dilatant breccias (hydraulic breccias) suggesting a hydrostatic stress state ($\sigma_1^* = \sigma_2^* = \sigma_3^* = -T$). (A) Saw-cut hand sample showing dark green serpentinite fragments cemented by white calcite along a paleo-detachment fault, Schistes Lustrés Zone, Queyras serpentinite, French Alps. Width of photograph: 25 cm. (B) River bed exposure of a dilatant breccia composed of low-porosity sandstone fragments (grey color) cemented by quartz (white color) along a vertical fault (white arrows), Oligocene Hyuga Group, Shimanto accretionary prism, Japan. (C) Saw-cut sandstone hand sample from nearby (B) exposure. Width of photograph: 15 cm.

Figure 5. Calcite-filled mode I and hybrid mineralized fractures associated with conjugate faults (arrows). The fractures are perpendicular to the steeply dipping bedding surface. Cretaceous limestones, Pyrenean foreland, Corbières, France (height of photograph: 2 m).

Figure 6. Mode I quartz-filled fracture in low-porosity Oligocene sandstones, Shimanto accretionary prism, Japan. The quartz fibers show an S shape, suggesting a component of displacement parallel to the fracture. Thickness of the vein: 15 mm.

Shear fractures result from a combination of extension and shear (hybrid failure). They classically form conjugate systems of *en échelon* fractures (Figure 5), where the long axis of the mineral fibers indicates the combination of extension and shear (Figure 6).

2.3. *Fracture reactivation vs. fracture neoformation*

Unlike in laboratory experiments, rock masses in the brittle crust are fractured. Therefore, it is not the intact rock strength that will dictate the stability of rock masses, but rather the strength of discontinuity (fault or fracture) surfaces [Byerlee, 1978]. Intact rock rupture criteria are replaced by more realistic *reactivation* criteria. The simplest and most widely used criterion is the Mohr–Coulomb reactivation criterion [Handin, 1969], quite similar to the Mohr–Coulomb criterion for the intact rock, and which can be written as

$$\tau = \mu\sigma_n + C.$$

The criterion postulates that the stability of fractured rock masses in the brittle crust is controlled by two basic parameters that can act in concert: (1) the coefficient of friction μ of the rock in contact or of the material filling the space between the two slipping surface walls, if any (e.g., fault gouge); (2) the normal stress component σ_n, acting perpendicularly to the discontinuity surface. The cohesion C is usually assumed to be equal to zero, given its negligible value for most rocks. Handin [1969] showed experimentally that if a pre-existing fracture is unfavorably oriented with respect to the principal stress axes, a new fracture with a more favorable orientation will form, leaving the pre-existing one unreactivated. This can be illustrated by a construction in the Mohr diagram (Figure 2c) where the Mohr circle tangents the intact rock failure envelope before the point corresponding to the pre-existing fracture reaches the reactivation envelope.

2.4. *The reactivation of moderately to severely misoriented fault surfaces*

In the brittle crust, the experimentally demonstrated preference of fracture neoformation over preexisting misoriented fracture reactivation does not seems to be a general rule. Indeed, in many instances, moderately to severely misoriented fault surfaces are reactivated, while no propagation of new surfaces is observed. Several mechanisms are proposed to solve this paradox, among which the most frequently invoked are as follows.

(1) The fault zone consists of a continuous layer of weak rocks, for instance rocks whose rheology can be regarded as plastic, visco-elastic, or elasto-plastic. This is the case with clay-rich or evaporite-rich strata (so-called décollement layers). Such a weak and continuous décollement layer will allow the displacement of allochton units over significant distances whatever the orientation of the fault zone with respect to the stress axes is favorable or not [Davis and Engelder, 1985, Weijermars et al., 1993, Costa and Vendeville, 2002, Vendeville et al., 2017].

(2) The fault surface is coated by low-friction ($\mu < 0.2$) material such as low-friction clay (e.g., montmorillonite) or talc [Morrow et al., 1992, 2017, Moore and Lockner, 2011, Boutareaud et al., 2012, Chen et al., 2017]. Leaving aside the stress corrosion process mentioned above, which concerns the nucleation of a mesoscopic fracture rather than reactivation of a macroscopic fracture or fault, fluids can weaken a fault by chemically reacting with the rocks or minerals along the damage zones or core zones of the fault. The chemically produced minerals can be frictionally weaker (so-called reaction softening). Examples of chemical weakening of fault rocks are described by White and Knipe [1978], Evans and Chester [1995], Wintsch et al. [1995], Gueydan et al. [2003], Collettini and Holdsworth [2004], Matsuda et al. [2004], Jefferies et al. [2006], Moore and Rymer [2007], Collettini et al. [2009b]. As indicated above, this reaction-softening effect will not be developed here.

(3) Along long-lived mature faults, damaged rocks inside the fault zone get their mechanical constants, such as their Young moduli or Poisson ratios, modified [Faulkner et al., 2006]. These modifications lead to a rotation of the stress axes in the vicinity of the fault [Healy, 2008]. The angle between σ_1 and the fault surface can thus be decreased and a very unfavorably oriented fault can become favorably oriented for reactivation. The studies of Provost and Houston [2001], Hardebeck and Michael [2004], Famin et al. [2014] suggest that vertical or steeply dipping strike-slip faults such as the San Andreas fault in California or the Median Tectonic Line in Japan can be reactivated following a rotation of the horizontal σ_1 axis to a more favorable value.

(4) The last mechanism, which is the main purpose of this paper, calls for the development of abnormally high p_f, which will decrease the normal stress σ_n to the effective σ_n^* [Hubbert and Rubey, 1959, Chapple, 1978]. The analysis of Sibson [1985],

which considers only the role of abnormally high p_f, without taking into account the role of the three other mechanisms, distinguishes three classes of fractures: (1) surfaces *favorably oriented* with respect to the stress axes, which can be reactivated with a hydrostatic p_f for given differential stresses (see oblique dashed black lines and point A, Figure 3); (2) surfaces *moderately misoriented* with respect to the stress axes that will require large differential stresses or suprahydrostatic p_f to be reactivated; (3) *severely misoriented* surfaces that will require, to be reactivated, p_f values larger than in cases (1) or (2), with $\sigma_3^* < 0$ (see oblique black lines on Figure 3). The maximum differential stress allowing reactivation of severely misoriented surfaces is limited by the failure envelope. If the differential stress gets too high, a new and more favorably oriented shear surface or a vein will form instead of reactivating the severely misoriented surface (points B and C on Figure 3). In all cases, for a given value of differential stress, the p_f value required to reactivate a severely misoriented surface is higher than that necessary for reactivation of a favorably oriented surface. The tectonic regime also has an impact on the λ values for reactivation and vein formation. Indeed, reverse tectonic regimes generally require higher p_f than normal stress regimes do (Figure 3).

2.5. *The fault valve model*

The *fault-valve* model, which is a consequence of the stress analysis of Sibson [1985], is based on the existence, in faulted regions, of fault planes moderately or severely misoriented with respect to the stress axes at the time of the fault activity [Sibson et al., 1988, Sibson, 1989, 1990]. The model is based on the following assumptions: (1) the coefficient of friction on the preexisting (misoriented) fault is of "Byerlee" type, that is, its value is between 0.6 and 0.85; (2) the cohesion C of the surface is neglected; (3) the fluid does not chemically react with the rock, that is, only the fluid pressure p_f plays a role.

The typical fault-valve behavior of a fault or fault system involves cyclical variations of p_f. A cycle consists of four stages: (1) p_f increases up to suprahydrostatic values below a hydraulic barrier, (2) rupture of the fault plane following a Mohr–Coulomb type criterion [Sibson, 1985], (3) fluid escape (upward or sideward) following increase of the rock permeability by fracturing and cataclasis associated with fault and hydraulic barrier ruptures, (4) fracture or pore sealing by mineral precipitation due to the sudden decrease of p_f down to hydrostatic values. This last stage eventually results in a restauration of the former seal, thus bringing back the faulted rock mass to a state before stage (1), allowing a repetition of the cycle. Following the initial discovery of this mechanism in mesothermal gold-quartz deposits by Sibson et al. [1988], this behavior was recognized in ancient fault systems [Cox, 1995, Robert et al., 1995, Hacker, 1997, Nguyen et al., 1998, Sibson and Scott, 1998, Faleiros et al., 2007]. The extensive damage to the rocks adjacent to the faults suggests that reactivation might have been seismogenic. The fault-valve model is proposed to account for present-day seismic reactivation of unfavourably oriented faults (see Section 4).

2.6. *The seismic pumping mechanism*

Seismic pumping provides a mechanism of formation of zoned mineralized veins along faults in the brittle crust by calling for fluid flow during earthquakes [Sibson et al., 1975, Kerrich et al., 1987]. The mineral zonation is interpreted as the result of repeated arrivals of fluids, each arrival leaving an imprint in the vein. In the pre-seismic stage, due to tectonic loading along the fault, dilatant structures such as tension cracks will create voids along and near the fault, aspirating nearby fluids. In the post-seismic stage, fluids will be expelled upwards or sidewards, before the cycle starts again. In itself, the seismic pumping mechanism does not increase directly the p_f value, but contributes to it by injecting volumes of fluids from remote areas towards active fault zones. It can also be active during diagenesis in faulted sedimentary basins [Wood and Boles, 1991].

2.7. *Shear stress-enhanced compaction*

In most cases, the central part, or core, of a fault zone is constituted by a weak material (clayey gouge, poorly consolidated breccia and so on). When tectonically loaded, a core material may undergo more compaction than the stronger surrounding rocks (damage zone, country rocks). If the core zone is (i) saturated by fluids and (ii) sealed (i.e., the fluid cannot escape), then tectonic load-induced compaction will increase p_f [Byerlee, 1990, Blanpied et al., 1992, Sleep and Blanpied, 1992]. The p_f increase will then decrease the effective normal stress σ_n^*, therefore allowing or favoring fault slip. Note that this mechanism does not require any temperature increase.

2.8. *Thermal pressurization*

Thermal pressurization, also called "dynamic" pressurization, concerns thin (a few millimeters to a few centimeters) fault core zones which are the site of coseismic slip along faults in the upper crust [Sibson, 1973, Lachenbruch, 1980, Mase and Smith, 1987, Wibberley and Shimamoto, 2005]. The phenomenon is based on a contrast between the thermal expansion of aqueous fluids trapped in the very-low-permeability fault core rock (clayey gouge in most cases) and the thermal expansion of the fault core rock matrix itself. During co-seismic, slip, the fluid-saturated rock will thermally expand due to shear heating, but fluids will expand in larger proportions than the pores. As long as the rock permeability remains low (e.g., in the absence of fracturing), the fluid cannot escape from the core zone and, following expansion, its pressure will increase drastically, resulting in a decrease of the normal stress acting on the surface.

The recognition of thermal pressurization processes during earthquakes or in the geological record is a challenge and, in addition to observations of natural microstructures [Ujiie et al., 2007, 2010, Boullier et al., 2009, Boullier, 2011], must rely on experimental reproduction of seismic slip and on numerical modeling [Noda and Shimamoto, 2003, Segall and Rice, 2006, Ujiie et al., 2011, Boutareaud et al., 2008, Ferri et al., 2010, Kitajima et al., 2011, Viesca and Garagash, 2015]. In addition to thermal pressurization strictly speaking, frictional heating can also lead to thermal decomposition of minerals such as phyllosilicates or carbonates (calcite, siderite), resulting in the release of fluids (H_2O, CO_2) that can then be pressurized [Brantut et al., 2008, 2010, Hirono et al., 2008, Ferri et al., 2010, Jeanne et al., 2014]. Frictional melting of the fault surface during co-seismic slip in carbonate-rich rocks can also result in a release of large amounts of CO_2 following volatile exsolution from the melt [Famin et al., 2008]. In the thermal decomposition or exsolution processes, the released fluids are considered to be pressurized and can consequently decrease the normal stress acting on the faults. Some authors contend that so-called injected cataclasites or injected gouges may result from co-seismic thermal pressurization [Lin et al., 2013, Lin, 2019].

3. Role of abnormally high p_f in crustal tectonics

3.1. *Role of abnormally high p_f in thrust tectonics*

In areas dominated by thin-skinned tectonics, thrust faults can accommodate significant (>10 km) horizontal displacements. To overcome the mechanical resistance of the allochtonous units to displacement, two mechanisms among the ones described above are frequently called for. The first mechanism (the translation made possible by weak ductile décollement layers) allows to account for the formation of several foreland thrust-and-fold belts such as the French-Swiss Jura belt or the Iranian Zagros belt [Jordan, 1992, Sherkati et al., 2006, Sommaruga et al., 2017, Lacombe and Mouthereau, 2002].

The other mechanism, that is, the translation of thrust sheets triggered or favored by supra-hydrostatic p_f, is inferred or ascertained in various tectonic settings. Table 1 provides examples of studies that call for supra-hydrostatic p_f to account for horizontal displacements along thrusts in collision belts or foreland fold-and-thrust belts. The supra-hydrostatic p_f lowers σ_n^*, thereby reducing the frictional resistance to motion and allowing a smooth displacement of the allochton units over their relative autochthonous basement. Evidence for supra-hydrostatic p_f either come from direct methods, namely p_f measurements in exploration boreholes, or from indirect methods, such as analyses of geological structures (e.g., dilatant crack-seal veins or implosion breccias) or modeling (critical Coulomb wedge, Coulomb stress change). Fluid inclusions preserved in mineralized veins can provide estimates of p_f at the time of vein formation. As such, they are a powerful and reliable method for p_f estimates.

The role of supra-hydrostatic p_f build-up appears critical or ubiquitous in accretionary prisms, whatever active or inactive [Moore and Vrolijk, 1992].

Table 1. Examples of geological or geophysical evidence for displacement along low-angle reverse faults triggered or favored by supra-hydrostatic pore fluid pressures p_f inside or near fault zones in collision belts or foreland fold-and-thrust belts, with pore fluid ratio λ estimates where available

Area	Name of structure	Evidence
Central Alps	Glarus thrust	Fracturing, veining, brecciation alternating with ductile deformation ($\lambda > 1$)[1]–[4]
Western Alps	Helvetic Diablerets nappe basal thrust	Large amounts of connate and metamorphic waters expelled upward, as indicated by $\delta^{18}O$, $\delta^{13}C$ and δD in calcite or quartz veins, possibly overpressured by rapid tectonic burial[5]
	Sub-Alpine frontal thrust zone (Chartreuse and Vercors) and foreland (Valence basin)	p_f measurements in exploration boreholes[6]
Pyrenees	Gavarnie thrust and splay faults	Fluid inclusions in quartz veins indicate fluctuations of p_f between lithostatic (~500 MPa) and hydrostatic (~200 MPa)[7]; combination of shear reactivation and extension vein opening ($\lambda = 0.77$–0.89)[8]
Himalaya	Himalayan Main Central Thrust	Critical Coulomb wedge modeling suggests $\lambda = 0.8$–0.9[9], Coulomb stress change modeling suggests $\lambda = 0.3$–0.9[10]
Apennines	Apenninic basal thrust zone, Apenninic foreland	Fluid inclusions in quartz veins indicate near-lithostatic p_f at the time of the emplacement of the Liguride nappes[11]; calcite-cemented implosion breccias filling dilational jogs ($p_f > \sigma_3$)[12]
Taiwan	Taiwan fold-and-thrust belt basal decollement fault, Chelungpu fault	p_f measurements in exploration boreholes ($\lambda \sim 0.7$)[13], critical Coulomb wedge modeling[14],[15]; discrete hydraulic fractures[16]
Western California	Coast Ranges and western Great Valley	p_f measurements in exploration boreholes[17],[18]

References: [1]Burkhard et al. [1992], [2]Badertscher and Burkhard [2000], [3]Badertscher et al. [2002], [4]Hürzeler and Abart [2008], [5]Crespo-Blanc et al. [1995], [6]Deville [2021], [7]Henderson and McCaig [1996], [8]Lacroix et al. [2013], [9]Mugnier et al. [1994], [10]Cattin and Avouac [2000], [11]Mullis [1988], [12]Vannucchi et al. [2010], [13]Suppe and Wittke [1977], [14]Davis et al. [1983], [15]Barr and Dahlen [1990], [16]Boullier [2011], [17]Melchiorre et al. [1999], [18]Unruh et al. [1992].

Table 2 provides examples of various continental margins or paleo-margins in which displacement along past or present (first-order) décollement faults or second-order faults (also referred to as splay faults) branching on décollements was or is possible due to supra-hydrostatic p_f. Similarly to what is inferred along large-displacement thrusts, the supra-hydrostatic p_f lowers σ_n^*, thereby reducing the frictional resistance to motion and allowing a smooth displacement of the overriding plate oceanwards, at least in the shallowest parts of the plate interface, before pressure and temperature increases lead to dehydration and expulsion of fluids. Direct evidence for supra-hydrostatic p_f along the basal décollements of accretionary prisms come form p_f measurements in Deep-Sea Drilling Project (DSDP), Ocean Drilling Program (ODP) or Integrated Ocean Drilling Program (IODP) boreholes. Porosity measurements

Table 2. Examples of geological or geophysical evidence for supra-hydrostatic pore fluid pressures p_f measured or inferred along low-angle reverse faults in accretionary prisms

Type of prism	Area	Type of structure	Evidence
Active accretionary prisms	Cascadia margin Oregon accretionary prism	Frontal décollement	Seismic velocity variations and negative polarity reflections in seismic profiles[1]–[3]; ODP core consolidation tests and logging data ($\lambda = 0.88$–0.99)[4]; supra-hydrostatic p_f ($\lambda = 0.8$) computed from velocity-depth data[5]; reverse polarity reflections from the décollement[6]
	Central America Costa Rica and Guatemala margins	Frontal décollement	Direct measurement of p_f in DSDP boreholes ($\lambda = 0.25$–0.48)[7]; consolidation tests on ODP cores suggest excess p_f (1.3–3.1 MPa)[8]; numerical modeling of p_f build-up following sediment dewatering in undrained conditions[9]; p_f measurements in ODP borehole hydrologic observatories ($\lambda = 0.25$–1)[10]; pervasive veining suggests p_f fluctuations in accordance with the seismic cycle[11]
	SW Japan Nankai Trough accretionary prism	Frontal décollement	Shear tests on saturated clay samples from the décollement indicate that friction drops dramatically with increasing p_f[12]; overconsolidation and dilatant fractures along the décollement[13]; seismic reflection amplitude variations along the décollement[14]; modeling of p_f based on acoustic velocity logs[15]; modeling of p_f based on laboratory permeability measurements from core samples suggest $\lambda^* = 0.68$–0.77[16]; supra-hydrostatic p_f deduced from seismic interval velocities[17]; empirical relationships between V_P, porosity, and effective σ_m obtained from laboratory deformation tests on drill core samples indicate excess p_f of 17–87 MPa[18]; upward flow of drilling mud from IODP borehole indicates an initial excess p_f of ~5–10 MPa above p_H[19]; estimation of p_f from empirical relationships between p_f, porosity and V_P, obtained from consolidation experiments and from drilling or sonic velocity data[20]
		Splay fault	High-amplitude negative polarity reflections in seismic profiles[21],[22]; low impedance layer[23]
	Lesser Antilles Barbados Ridge accretionary prism	Frontal décollement	p_f estimated from seismic velocity or from negative polarity reflections[24],[25]; direct measurements in ODP boreholes and sediment consolidation tests (λ up to >0.9)[26],[27]; high p_f suggested by anisotropy of magnetic susceptibility[28]
	New Zealand Hikurangi accretionary prism	Pāpaku splay fault	Rock deformation experiments on cores from the fault zone ($\lambda^* = 0.3$–0.6)[29]

(continued on next page)

Table 2. (continued)

Type of prism	Area	Type of structure	Evidence
Exhumed inactive accretionary prisms	Shimanto accretionary prism (Japan)	Nobeoka paleo-décollement	Fluid inclusions and modeling suggest p_f excess values between 5 and 20 MPa[30]
		Nakanomata splay fault	Quartz-cemented syntectonic dilatant hydraulic breccias[31]
	Kodiak accretionary prism (Alaska)	Paleo-décollements and mélange zones	Crack-seal quartz veins parallel to ancient decollements interpreted as resulting from repeated hydrofracturing ($p_f > \sigma_3$)[32]; fluid inclusions indicate near-lithostatic p_f ($p_f \sim \sigma_1$) at the time of quartz vein formation[33],[34]; lack of low-friction material and mechanical analysis of displacement along the décollement plead for supra-hydrostatic p_f[35]; hydrofractures suggest supra-hydrostatic p_f[36]; fluid inclusions in hydrofractures suggest near-lithostatic p_f[37]
	Chrystalls Beach accretionary prism (New Zealand)	Mudstone matrix of mélange	Shear veins severely misoriented with respect to stress field[38],[39]

References: [1]Cochrane et al. [1994], [2]Cochrane et al. [1996], [3]Moore et al. [1995a], [4]Moore et al. [1995b], [5]Hyndman et al. [1993], [6]Tobin et al. [1994], [7]Von Huene [1985], [8]Saffer et al. [2000], [9]Screaton and Saffer [2005], [10]Davis and Villinger [2006], [11]Vannucchi and Leoni [2007], [12]Brown et al. [2003], [13]Ujiie et al. [2003], [14]Bangs et al. [2004], [15]Tsuji et al. [2008], [16]Skarbek and Saffer [2009], [17]Tobin and Saffer [2009], [18]Kitajima and Saffer [2012], [19]Hirose et al. [2021], [20]Pwavodi and Doan [2024], [21]Park et al. [2000], [22]Park et al. [2002], [23]Bangs et al. [1990], [24]Shipley et al. [1994], [25]Moore et al. [1995c], [26]Moore and Tobin [1997], [27]Moore et al. [1998], [28]Housen et al. [1996], [29]French and Morgan [2020], [30]Raimbourg et al. [2015], [31]Passelègue et al. [2014], [32]Fisher and Byrne [1987], [33]Vrolijk [1987], [34]Vrolijk et al. [1988], [35]Byrne and Fisher [1990], [36]Fisher et al. [1995], [37]Rowe et al. [2009], [38]Fagereng et al. [2010], [39]Fagereng et al. [2011].

ODP: Ocean Drilling Program. IODP: International Ocean Drilling Program. 3D: three-dimensional. p_H: hydrostatic pressure. σ_m: mean stress ($\sigma_m = (\sigma_1+\sigma_2+\sigma_3)/3$). λ^*: modified pore fluid factor, $\lambda^* = (p_f - p_H)/(p_L - p_H)$, where p_H is the hydrostatic pressure and p_L the lithostatic pressure caused by the weight of the overburden [Saffer and Tobin, 2011].

and various mechanical tests (e.g., consolidation tests) on DSDP/ODP/IODP cores further testify for under-compaction of sediments or rocks along the décollements, accounted for by the assumption of supra-hydrostatic to nearly lithostatic p_f. The presence of hydrofractures along as well as above or below décollements is also direct evidence [Table 2; see also Behrmann, 1991]. Indirect evidence come from seismic reflection imaging, with characteristic negative polarity reflections along décollement surfaces. Lastly, the weakening role of supra-hydrostatically pressurized fluids along the basal décollement of accretionary prisms can be reproduced by analog modelling [Cobbold et al., 2001, Mourgues and Cobbold, 2003].

3.2. *Role of abnormally high p_f in extensional tectonics*

Large displacement along low-angle normal faults, also referred to as detachments, is mechanically paradoxical. The different mechanisms mentioned above to account for the displacement along misoriented fault surfaces apply to low-angle normal faults [Reynolds and Lister, 1987, Yin, 1989, Axen, 1992, Westaway, 1999, Abers, 2009, Collettini, 2011]. Table 3 provides examples of studies which suggest or demonstrate that reactivation of low-angle normal faults was possible because of supra-hydrostatic to lithostatic p_f values. Regarding inactive detachments, structural evidence for high p_f come from textures of precipitated minerals in breccia cements (so-called cockade structures) or in flat-lying crack-seal dilatant veins. Fluid inclusions in the precipitated minerals also provide indications. Lastly, mechanical modeling also accounts for overpressured-fluid-aided displacements along low-angle faults. Regarding active detachments, evidence consist of vein or breccia cement texture analyses (including fluid inclusions), mechanical modeling, p_f measurements in boreholes, geophysical investigations (body wave velocity anomalies).

The other mechanisms listed above may also facilitate large displacement along low-angle normal faults. In particular, analog modeling suggests that extension can take place above continuous low-strength layers such as evaporites [Vendeville and Jackson, 1992a,b]. Regarding the reorientation of the stress axes in the vicinity of the fault, Lecomte et al. [2011] propose to explain reactivation of misoriented low-angle normal faults by calling for an elasto-plastic frictional gouge instead of the classical frictional fault gouge. Plastic strain can initiate the displacement despite the misorientation. Following the initiation, stress axes near the fault zone rotate to a more favorable orientation with respect to the fault surface, allowing further displacement.

3.3. *Role of abnormally high p_f in strike-slip tectonics*

The activity of steeply dipping to vertical plate-boundary transform or intra-plate strike-slip faults moderately to severely misoriented with respect to the principal stress axes constitutes a challenge since the discovery of nearlyperpendicular normal stresses acting along the San Andreas fault [Mount and Suppe, 1987, Zoback et al., 1987]. As such, the San Andreas faults appears as a weak fault, and explanations for it have been extensively looked for. The models and mechanical analyses of Byerlee [1990, 1993] and Rice [1992] attempt to show that supra-hydrostatic p_f could account for the weakness of the fault. Experimental measurement of clay permeabilities [e.g., Faulkner and Rutter, 2001] provide a mechanism for the maintenance of excess p_f in strike-slip fault zones. However, drilling across the fault zone during the SAFOD (San Andreas Fault Observatory at Depth) program at ~3 km depth did not reveal any supra-hydrostatic p_f, prompting researchers to propose other mechanisms that could explain the weakness: fault rocks with extremely low friction coefficients such as talc [Moore and Rymer, 2007] or clays [Schleicher et al., 2009a,b, Carpenter et al., 2011, Holdsworth et al., 2011], stress axes reorientations to more favorable attitudes at short distances from the fault [Provost and Houston, 2001, Hardebeck and Michael, 2004, Healy, 2008]. It seems clear that pressurized fluids do not weaken the San Andreas fault in its upper part (between the surface and a ~3 km depth), except perhaps for micro-earthquake activity [Mittempergher et al., 2011]. Hydro-mechanical modeling [e.g., Fulton and Saffer, 2009, Beeler et al., 2013] suggests that supra-hydrostatic p_f could play a role in the weakening at depths larger than the SAFOD drilling. Conversely, hydro-mechanical modeling by Fulton et al. [2009] suggest that supra-hydrostatic p_f cannot

Table 3. Examples of geological or geophysical evidence for displacement along low-angle normal faults (detachment faults) triggered or favored by supra-hydrostatic pore fluid pressures p_f inside or near the fault zone

Type of low-angle normal fault	Name of structure, area	Evidence
Inactive intra-continental	Western US Basin and Range (Southern Mountains MCC deformed zones, Arizona; Whipple detachment, California; Siever Desert detachment, Utah)	Flat-lying dilatant veins suggest $p_f > \sigma_3$[1]; fluid inclusions in quartz veins suggest $p_f \geq 120$ MPa[2],[3]; critical Coulomb wedge analysis suggests $p_f \sim 0.6\,\sigma_v$[4]
	Central Alps (Brenner, Simplon and Grimsel faults)	Fluid inclusions in veins suggest supra-hydrostatic p_f[5]; mylonitic zone embrittlement suggests episodic supra-hydrostatic p_f[6],[7]; textural characteristics of cockade structures in a fault breccia and mechano-chemical calculations allow to reconstruct p_f fluctuations related to different stages of the seismic cycle[8]
	Gulf of Corinth LANF, Greece	Limit Analysis (maximum strength theorem analysis) suggests $p_f = 0.57$–$0.77\,\sigma_v$[9]
Active intra-continental	North Apennines LANFs, including Alto Tiberina and Tellaro detachments	Limit Analysis (maximum strength thorem analysis) suggests that $p_f = 0.57$–$0.77\,\sigma_v$[9]; $p_f \sim 0.85\,\sigma_v$ in exploration boreholes[10]; brittle tensile structures and fluid inclusions in calcite veins suggest episodic supra-hydrostatic p_f[11]; V_P positive anomaly, V_P/V_S negative anomaly[12]
Inactive intra-oceanic or intra-OCT	Detachment surfaces exposed in Alpine ophiolites	Calcite-cemented breccias (ophicalcites)[13],[14]; gouge veins injected in cataclasite suggest transient supra-hydrostatic p_f[15]
Active intra-oceanic	Mid-Atlantic ridge Atlantis massif, mid-Atlantic ridge 13°–15° N	Fluid inclusions[16],[17]; hydraulic breccias[18]
	South Pacific Woodlark-D'Entrecasteaux ridge Moresby detachment	Low V_P and high porosity values in the fault zone suggest supra-hydrostatic p_f[19]; dilatant crak-seal veins suggest episodic near-lithostatic p_f and hydrofracturing[20],[21]; calcite veins parallel to foliation suggest supra-lithostatic p_f[22]

References: [1] Reynolds and Lister [1987], [2] Smith et al. [1991], [3] Selverstone et al. [2012], [4] Yuan et al. [2018], [5] Selverstone et al. [1995], [6] Axen et al. [1995], [7] Axen et al. [2001], [8] Berger and Herwegh [2019], [9] Yuan et al. [2020], [10] Collettini et al. [2008], [11] Clemenzi et al. [2015], [12] Moretti et al. [2009], [13] Früh-Green et al. [1990], [14] Picazo et al. [2013], [15] Manatschal [1999], [16] Escartin et al. [2003], [17] Castelain et al. [2014], [18] Picazo et al. [2012], [19] Floyd et al. [2001], [20] Roller et al. [2001], [21] Kopf et al. [2003], [22] Famin and Nakashima [2005].

MCC: metamorphic core complex. LANF: low-angle normal fault. OCT: ocean-continent transition. σ_v: principal vertical stress axis.

be maintained along the San Andreas fault at shallow (<3 km) depth, and that other mechanisms such as shear-enhanced compaction or thermal pressurization inside the fault zone have to be invoked.

Table 4 provides examples of transform or strike-slip faults along which supra-hydrostatic p_f could play or could have played a role in the past or present fault activity. Direct evidence for abnormally high p_f can be found in shallow boreholes drilled across the New Zealand Alpine fault, but no data from depths larger than a few hundred meters are available. Indirect evidence consist either in rare hydraulic fractures or in more frequently observed geophysical (electrical conductivity or seismic velocity) anomalies. In this last case, even if the anomalies can be interpreted as caused by the presence of fluids at depth, they do not bring undisputable evidence for pressurized fluids. The apparent scarcity of abnormally high p_f ascertained along transform or strike-slip fault zones may be due to the lack or scarcity of efficient seals. Indeed, fault zones, especially their damage zones if any, crossing the entire crust may appear as conduits rather than barriers or seals.

3.4. *Conclusions*

A review of the literature dealing with the role of abnormally high p_f along faults in the brittle crust allows to draw the following key ideas.

(1) Undebatable evidence for supra-hydrostatic p_f come from pressure measurements in oil industry or scientific boreholes (DSDP, OPD, IODP). Near-horizontal dilatant veins found along low-angle faults also constitute a strong evidence, especially when fluid inclusions preserved in these veins indicate supra-hydrostatic p_f at the time of fluid entrapment. Geophysical anomalies, either electrical (conductivities) or seismological (seismic velocities), are interpreted as caused by abnormally high p_f at depth along fault zones.

(2) Evidence, whatever direct or indirect, for supra-hydrostatic p_f appear common along low-angle normal faults (detachments) or reverse faults (including décollements) (Tables 1–3). Fluids appear to be efficiently trapped beneath flat-lying or gently dipping allochtons that can act as impervious or low-permeability lids. Conversely, conclusive evidence for supra-hydrostatic p_f along transform or strike-slip faults are scarcer than along low-angle normal or reverse faults (Table 4), possibly because such vertical or steeplydipping fault zones lack tight and laterally continuous seals that could prevent fluids from leaking upward to the surface.

(3) Along with fracturing and comminution linked with displacement along faults, fluid circulation and associated fluid-rock interactions quite often result in alteration of minerals, resulting in weaker minerals such as clays, talc and other minerals whose frictional properties are much weaker than primary minerals. This chemical effect of fluids is clearly a serious competitor with the pressurization of fluids to account for fault weakening.

(4) Mechanisms such as shear stress-enhanced compaction, thermal pressurization, or stress reorientation near fault zones certainly play roles in the reactivation of misoriented faults, but they are difficult to be recognized in the geological record.

4. Fluids and natural earthquakes

4.1. *Intra-plate earthquakes, earthquake sequences, background seismicity, subduction earthquakes*

Table 5 presents examples of studies that attempt to relate major intra-continental earthquakes, earthquake sequences, background seismicity, subduction earthquakes and aftershock sequences to abnormally high p_f. Some of these examples were already introduced in the previous section, but without any specific mention to the seismogenic activity of the relevant faults.

Except rare examples of direct measurements in boreholes, evidence for supra-hydrostatic p_f triggering or favoring intra-plate earthquakes are mostly indirect. Body-wave velocity anomalies detected by two-dimensional or three-dimensional tomography suggest that pressurized fluids are present in hypocentral regions of many earthquakes. Most authors agree that fluids are trapped at depth and that their accumulation results in abnormally high p_f values which in turn weaken the faults.

Evidence for abnormally high p_f that could either trigger or favor the propagation of subduction zone earthquakes mainly comes from body wave velocity anomalies revealed by tomography (Table 5). Other indirect evidence come from mechanical analyses based on the reactivation of misoriented fault

Table 4. Examples of geological or geophysical evidence for displacement along transform faults or strike-slip faults triggered or favored by supra-hydrostatic pore fluid pressures p_f inside or near fault zones

Area, name of structure	Evidence
California, San Andreas fault	Very low resistivity, low V_P, and high a V_P/V_S ratio suggest supra-hydrostatic p_f[1]; calcite and anhydrite-filled mode I veins in SAFOD cores suggest that transient increases of supra-hydrostatic (possibly supra-lithostatic) p_f occurred during fault activity and may constitute a triggering mechanism for some micro-earthquakes recorded at depth near SAFOD drilling site[2]; frictional sliding and stress-driven DMT microstructures suggest that deformation in the active shear zones is displacement-weakening, possibly due to local and transient high p_f build-ups along creeping segments[3]; microstructural and geochemical data from SAFOD samples indicate that transient co-seismic fluid overpressure events overprint aseismic creep along the fault[4]
Turkey, North Anatolian Fault	Fluid inclusions in subhorizontal extension veins suggest supra-hydrostatic p_f[5]; continuous ascent of deep crustal or mantle fluid (CO_2, CH_4 or He) could result in near-lithostatic or supra-lithostatic p_f[6]; low electrical resistivity (measured by magnetotelluric methods) and low V_P (measured by 2-D seismic velocity tomography) suggest high p_f at 5–15 km depth[7],[8],[9]
New Zealand, Alpine Fault	Slug tests in shallow (150 m deep) boreholes suggest that the near-surface Alpine fault zone may be site of high p_f gradient[10]; pressure measurement during drilling reveals a slight (9%) supra-hydrostatic p_f in shallow (~900 m deep) borehole[11]; tremors appear to be located at 25–45 km depth, in a region of high P-wave attenuation that could be the site of supra-hydrostatic p_f[12]
Japan, Atotsugawa fault	High p_f could account for creep along some parts of the fault[13]
Japan, Nojima fault	Discrete hydraulic fractures[14]
Central Alps, Adamello pluton	Reactivation of the severely misoriented inactive Gole Larghe fault[15]
Southeastern Brazil, Ribeira Shear Zone	Fluid inclusions in foliation-parallel or extensional quartz veins along the shear zone indicate p_f fluctuations that are interpreted as the result of a fault-valve behavior[16]

References: [1]Eberhart-Phillips and Michael [1993], [2]Mittempergher et al. [2011], [3]Hadizadeh et al. [2012], [4]Hadizadeh et al. [2024], [5]Janssen et al. [1997], [6]Pfister et al. [2000], [7]Karabulut et al. [2003], [8]Tank et al. [2005], [9]Karaş et al. [2020], [10]Sutherland et al. [2012], [11]Sutherland et al. [2017], [12]Wallace [2020], [13]Kato et al. [2007], [14]Boullier [2011], [15]Mittempergher et al. [2009], [16]Faleiros et al. [2007].

SAFOD: San Andreas Fault Observatory at Depth. DMT: diffusive mass transfert.

Table 5. Examples of geophysical evidence for major earthquakes and aftershocks triggered or favored by abnormally high pore fluid pressures p_f in or around fault zones

Type of event	Area and/or events	Evidence
Intraplate earthquakes, earthquake sequences and background seismicity	Central Alps	Unexpected background seismic activity in the lower crust accounted for by supra-hydrostatic p_f[1]
	Himalaya MCT	Drop in V_P and V_S values, increase of V_P/V_S[2]
	Himalaya background sesimicity	Supra-hydrostatic p_f at depth deduced from correlated seasonal variation of stress and seismicity[3]
	Northern Apennines (1997–1998 Umbria-Marche-Colfiorito, 2000 Faenza and 2012 Emilia seismic sequences)	Supra-hydrostatic p_f ($\lambda \geq 0.9$) inferred from the presence at depth of Triassic evaporite impervious seals[4]; supra-hydrostatic p_f ($\lambda \geq 0.7$) suggested by stress inversion of focal mechanisms[5]; space–time evolution of seismic activity fits with diffusion laws, $p_f \sim \sigma_V$[6],[7]; V_P/V_S changes along a fault system suggest that p_f fluctuations controlled the space–time evolution of the Emilia sequence and the activation of the second main shock[8]
	Central and southern Apennines (2009 Abruzzo-L'Aquila sequence, 2010–2014 Mt Pollino sequence)	Supra-hydrostatic CO_2 p_f values in exploratory boreholes[9],[10]; supra-hydrostatic p_f propagation along a fault system tracked by space–time variations of V_P/V_S anomalies during earthquake migration[11]; high V_P/V_S and low Q_P/Q_S indicative of supra-hydrostatic p_f[12]; temporal evolution of V_P/V_S suggests an increase through time of supra-hydrostatic p_f (up to ~200 MPa at 10 km depth), eventually triggering the 6 April 2009 M_W 6.3 mainshock[13]; increase of the V_P/V_S ratio and evolution of shear wave splitting before the earthquake are interpreted as reflecting the progressive influx of pressurized fluids near the hypocentral of the M_w 6.3 L'Aquila main shock[14]; mantle-sourced CO_2 accumulates under near-lithostatic or supra-lithostatic p_f in deep traps which may control the Apennines seismic activity[15],[16]
	East Iceland rift zone	Stress inversion of focal mechanisms suggests near-lithostatic p_f values ($\lambda \sim 1$)[17]
	Back-arc side of NE Japan ($M > 6$ thrust-fault type events)	Mohr–Coulomb analysis suggests that severely misoriented faults are reactivated by supra-hydrostatic p_f through a fault-valve mechanism[18]

(continued on next page)

Table 5. (continued)

Type of event	Area and/or events	Evidence
	Kaapvaal craton (2017 M_W 6.5 Bostwana earthquake)	Episodic seismic activity in an otherwise stable craton explained by sporadic near-lithostatic p_f ($\lambda \sim 0.85$)[19]
	New Madrid seismic zone (1811–1812 sequence)	A test of the role of stress tensor shape Φ, fault friction coefficient μ, p_f, and gradient of σ_D with depth by a Mohr–Coulomb-based parametric analysis shows that reactivation of the faults requires supra-hydrostatic p_f ($\lambda = 0.68$–0.81), unless μ is less than 0.4[20]
	Japan, Nojima fault, 1995 M_W 7.2 Kobe earthquake	Seismic velocity anomalies near the hypocenter could reflect supra-hydrostatic p_f that may have contributed to the initiation of the Kobe earthquake[21]
	Cascadia	Seismic tomography indicates abnormal V_P/V_S and Poisson ratio values interpreted as caused by near-lithostatic p_f[22],[23]
	NE Japan	Aftershock focal mechanisms of the 1968 M 8.2 Tokachi earthquake suggest a weak plate interface accounted for by the post-seismic release of overpressured fluids following the main rupture[24]; seismic reflection imaging shows that the megathrust corresponds to a reflector with negative polarity, which could be explained by high p_f having possibly triggered the the 2011 M_W 9 Tohoku event[25]; mechanical analysis suggests stress permutations in the forearc region caused by fluctuations in p_f during the seismic cycle (fault-valve action)[26]
	SW Japan	3-D seismic reflection data show the presence of a LVZ (~2 km thick, ~15 km wide, and ~120 km long) beneath the Nankai accretionary prism, inside which inferred abnormally high p_f may control interplate coupling[27]
	Central America	Extremely high V_P/V_S ratios in the entire subducting oceanic crust is interpreted as due to high p_f. Varying velocity ratios in the overriding continental crust further allow to map varying coupling domains[28]
	Chile	The importance of the post-seismic fluid discharge suggests overpressured p_f beneath the subduction interface before large interplate events[29],[30]; 3-D seismic tomography allows to map the distribution, along the plate interface, of domains with abnormally high p_f and domains with lower p_f and to propose a correlation between these domains and the patches which slip aseismically (high p_f) and those which are locked (low p_f)[31]

(continued on next page)

Table 5. (continued)

Type of event	Area and/or events	Evidence
Aftershocks	New Zealand, Hikurangi subduction zone	A Mohr–Coulomb analysis suggests that the recurrence of megathrust earthquakes may be triggered by fluctuation of p_f (from hydrostatic to lithostatic) in addition to stress accumulation[32]
	1992 Landers earthquake	Increase of p_f because of post-seismic fluid flow and Coulomb stress changes account for the chronology and spatial migration of the Landers event aftershocks[33]
	Apennines (1997 Umbria-Marche, 2009 L'Aquila, 2012 Emilia earthquake sequence)	Space–time migration of aftershocks fits with diffusion laws of fluids in porous media[34],[35]; inversion of earthquake nodal planes allows to map the 3-D p_f distribution at depth in the hypocentral region of the L'Aquila earthquake and shows that time-space migration of aftershocks fits with diffusion laws of p_f[36]; aftershocks induced by a reduction in the fault shear strength due to a pulse of p_f[37]; aftershock decay rate and V_P/V_S changes along the fault system suggest that a p_f pulse controlled the space–time evolution of the 2012 Emilia sequence[38]
	2011 Tohoku earthquake, NE Japan	Reactivation of misoriented fault planes of the aftershock seismic faults is accounted for by varying supra-hydrostatic p_f[39]
	2004 Sumatra earthquake	Aftershock migration along a splay fault merging with the megathrust is explained by upward migration of fluids, although supra-hydrostatic p_f is not ascertained[40]

References: [1]Deichmann [1992], [2]Mandal et al. [2022], [3]Bettinelli et al. [2008], [4]Quattrocchi [1999], [5]Boncio and Bracone [2009], [6]Lombardi et al. [2010], [7]Calderoni et al. [2009], [8]Pezzo et al. [2018], [9]Collettini et al. [2009a], [10]Chiodini et al. [2004], [11]Chiarabba et al. [2009a], [12]Chiarabba et al. [2009b]), [13]Di Luccio et al. [2010], [14]Lucente et al. [2010], [15]Chiodini et al. [2011], [16]Di Luccio et al. [2022], [17]Plateaux et al. [2012], [18]Sibson [2007, 2009], [19]Gardonio et al. [2018], [20]Leclère and Calais [2019], [21]Zhao et al. [1996], [22]Audet et al. [2009], [23]Peacock et al. [2011], [24]Magee and Zoback [1993], [25]Kimura et al. [2012], [26]Sibson [2013], [27]Park et al. [2010], [28]Audet and Schwartz [2013], [29]Husen and Kissling [2001], [30]Koerner et al. [2004], [31]Moreno et al. [2014], [32]Sibson and Rowland [2003], [33]Bosl and Nur [2002], [34]Miller et al. [2004], [35]Antonioli et al. [2005], [36]Terakawa et al. [2010], [37]Malagnini et al. [2012], [38]Pezzo et al. [2018], [39]Leclère and Fabbri [2013], [40]Waldhauser et al. [2012].

MCT: Main Central Thrust. Q_P/Q_S: attenuation ratios of P and S waves. 3-D: three-dimensional. LVZ: low seismic velocity zone. Φ: stress tensor shape; $\Phi = (\sigma_2 - \sigma_3)/(\sigma_1 - \sigma_3)$.

planes [e.g., Sibson, 2013]. The analysis of Seno [2009], based on the construction of the differential stress profiles across several subduction zones, shows that the pore fluid pressure ratio λ accounts for much of the interplate coupling.

4.2. *Aftershocks*

4.2.1. *Present-day aftershocks*

In many cases, aftershocks following large magnitude events typically migrate both in space and time. This was first noticed by Nur and Booker [1972] following the fortuitous or induced seismic sequences at Denver and Rangely [Healy et al., 1968, Raleigh et al., 1976]. Since then, precise hypocenter relocations show that the temporal and spatial migration follows laws of diffusion of pressure fronts in porous media, suggesting that pressurized fluids contribute to trigger aftershocks (Table 5). The theoretical analysis of Miller [2020], based on the modeling of permeability fluctuations with time during the seismic cycle, further shows that major events not characterized by co-seismic or post-seismic releases of large amounts of fluids are followed by very few aftershocks, whereas those characterized by the release of significant amounts of co- or post-seismic fluids will be followed by large aftershock populations. Even if other mechanisms such as loading of faults by Coulomb stress transfer can influence the triggering or the propagation of aftershocks [Nostro et al., 2005], the role of supra-hydrostatic p_f appears significant in many cases.

4.2.2. *Aftershocks in the geological record*

Because of their small magnitudes, aftershocks related to past earthquakes are uneasy to recognize in the geological record. However, a specific type of aftershocks, called "golden" aftershocks, is presumably recognized in Archean rocks (Yilgarn craton, western Australia) where mechanical analyses based on Coulomb stress transfer following major earthquakes suggest that transiently abnormally high p_f triggered ruptures on secondary faults after main events [Cox and Ruming, 2004, Micklethwaite, 2008]. Indeed, the Yilgarn craton gold deposits hosted in secondary low-displacement hectometric faults and shear zones do not show a random spatial distribution, but are clustered in rock volumes near terminations of primary plurikilometric strike-slip fault segments. Mechanical analyses of the stress transfer following major earthquakes along any of the fault segments show that specific rock volumes are stress-loaded ahead of the segment terminations [so-called "loaded" lobes, inside which the stress state acting on pre-existing fractures makes them close to failure; King et al., 1994]. Pressurized fluid expelled from the main shock hypocentral volume then percolates through the fracture network in the loaded lobes, triggering eventual ruptures and allowing, by pressure drop, deposition of gold-bearing mineralization. The repetition of main shocks and aftershocks eventually results in deposits of economical interest.

4.3. *Subducting slab intermediate-depth earthquakes*

4.3.1. *Seismological evidence for supra-hydrostatic p_f in currently subducting slabs*

In subduction zones, intermediate-depth earthquakes, that is, earthquakes with hypocentral depths between ~50 and 300 km, are no longer localized along the plate interface, but inside the subducting slab. Various mechanisms have been proposed to account for nucleation or propagation of this intermediate-depth seismicity [Frohlich, 2006, Houston, 2015]: (1) dehydration embrittlement, in which locally abnormally high p_f allows a transition from a viscous regime of deformation to brittle faulting, (2) thermal instabilities, or (self-localizing) thermal runaway, in which incipient ductile shear zones develop as rheological instabilities along which brittle failure can nucleate; (3) "anticrack faulting", triggered by mineral phase change reactions. Among these mechanisms, which can act in concert, the first one is of peculiar interest here. As summarized in Table 6, evidence or suspicion for supra-hydrostatic p_f come from three-dimensional seismic tomography across subducting slabs currently in their post-seismic stage or in their inter-seismic stage.

4.3.2. *Evidence for excess p_f at intermediate depths in the geological record*

Table 6 further provides examples of structures (crack-seal veins, mineral overgrowths) reported from high-pressure metamorphic terranes which

Table 6. Examples of geological and geophysical evidence for intermediate-depth seismicity in modern or fossil subduction zones triggered or favored by supra-hydrostatic pore fluid pressures p_f

Setting	Area	Name of structure	Evidence
	NE Japan	Japan trench (subducting Pacific slab)	Seismic tomography indicates abnormal V_P/V_S and Poisson ratio values interpreted as caused by near-lithostatic p_f[1]; seismic tomography shows slab dehydration; released fluids become overpressured and account for seismicity[2]; 3D seismic tomography suggests evidence for near-lithostatic p_f in the hypocentre of a M_W 7.1 intraslab earthquake at a 66 km depth[3]; V_P and V_S variations in the subducting slab indicates development of high p_f[4],[5]
	Central Andean subduction	Chile trench (subducting Nazca plate)	High p_f could have contributed to the nucleation or to the propagation of a M_W 7.8 earthquake in northern Chile at a 115 km depth[6]; high V_P/V_S ratios in the subducting Nazca plate and thermodynamic modeling of dehydration reactions suggest high p_f at depths >50 km[7]
	Lesser Antilles	Subducting Atlantic plate	Hypocenters between 120 and 160 km are distributed where seismic tomography indicates low V_P values and high V_P/V_S ratios, suggesting high p_f[8]
	Middle America trench	Middle America trench (subducting Cocos plate)	Nucleation of a M_W 7.1 earthquake at a 57 km depth in the subducting Cocos plate tentatively explained by high p_f resulting from the brucite + antigorite = olivine + H_2O reaction[9]

(continued on next page)

Table 6. (continued)

Setting	Area	Name of structure	Evidence
Fossil subduction zones	Central Alps	Dent Blanche basal thrust	Cross-cutting relationships between foliated cataclasites, mylonites and quartz-clinozoisite veins ($0.95 < \lambda < 1$)[10]
		Valpelline Shear Zone between Valpelline and Arolla units, Dent Blanche	Metamorphic tensile veins ($\lambda \sim 0.7$)[11]
	Western Alps	Monviso	HP crack-seal veins in eclogite-facies metagabbros and oscillatory growth zoning of minerals as products of precipitation suggest fluctuations of p_f[12]; eclogite-facies vugs suggest lithostatic p_f[13]; four distinct large negative δ^7Li excursions in garnet mantles result from kinetic fractionation of Li isotopes through bulk diffusion during at least four overpressured fluid pulses[14]
		Lanzo	Hydrofracturing of omphacitites by CH_4–H_2-rich fluids at 30–80 km depth[15]
	California	Franciscan Complex	Rhythmic chemical zoning in HP garnets result from growth-dissolution cycles driven by pressure pulses (p_f = 100–350 MPa)[16]
	Zambia	Relics of subducted lower oceanic crust, late Precambrian Zambezi belt	Hydraulic fracturing[17]

References: [1]Nakajima et al. [2001], [2]Mishra and Zhao [2004], [3]Nakajima et al. [2011], [4]Shiina et al. [2013], [5]Shiina et al. [2017], [6]Kuge et al. [2010], [7]Bloch et al. [2018], [8]Paulatto et al. [2017], [9]Gutiérrez-Aguilar et al. [2022], [10]Angiboust et al. [2015], [11]Menant et al. [2018], [12]Spandler et al. [2011], [13]Angiboust and Raimondo [2022], [14]Hoover et al. [2022], [15]Giuntoli et al. [2024], [16]Viete et al. [2018], [17]John and Schenk [2006].

HP: high pressure metamorphic conditions.

can be interpreted as resulting from overpressured fluids during intermediate-depth seismic activity. Brittle dilatant veins crossing ductilely deformed high-pressure rocks are one convincing piece of evidence for abnormally high p_f. Similarly, finely zoned rims around garnets in eclogitic rocks can be interpreted as repeated growths of thin garnet layers following cyclical arrivals of co-seismic fluids. In these cases, the sharpness of the boundaries between the domains with distinct element concentrations are sharp, whereas they should be irregular or diffuse in the case of intracystalline high-temperature solid diffusion, confirming the fluid pulse hypothesis. Through a detailed analysis of such zoned garnet overgrowths, Viete et al. [2018] estimate that at least four overpressured fluid pulses occurred in less than 300,000 years.

4.4. *Seismic swarms*

Whatever they are related to volcanic systems or not, many seismic swarms appear to be triggered or favored by pressurized fluids (Table 7). The most convincing argument for the role of p_f lies in the fact that, like for aftershock sequences, the spatial and temporal migration of hypocentres follows diffusion laws of pressure front propagation in porous media. Several authors however propose that other mechanisms can also play a role, in combination with p_f wave propagation. A frequently invoked additional mechanism is Coulomb stress transfer [Aoyama et al., 2002, Hainzl, 2004, Yukutake et al., 2011, Fischer et al., 2014]. In particular, studying a swarm developed near the Hakone volcano, central Japan, Yukutake et al. [2011] were able to show that the hypocenters of a first earthquake sequence were aligned along fault-like planar surfaces, while those of a subsequent sequence were located in compressive lobes associated with the planar surfaces, demonstrating the sequence fluid-triggered events followed by Coulomb stress transfer-triggered events. Besides, Aoyama et al. [2002] call for stress corrosion as an additional mechanism in the triggering of seismic swarms.

4.5. *Fluid overpressures and slow earthquakes*

Slow earthquakes, a collective name including slow-slip events, low- or very-low-frequency earthquakes, low-frequency tremors, non-volcanic tremors, and episodic tremor-and-slip events, are in many cases suspected to be triggered or favored by supra-hydrostatic p_f. Table 8 is a non-exhaustive compilation of studies that relate slow earthquakes (in the broad sense) with evidence for supra-hydrostatic p_f. With the exception of one study pertaining to the San Andreas fault, all other studies deal with slow earthquakes in subduction zones. Direct evidence come from measurements in ODP or IODP boreholes equipped with pressure or fluid flow sensors [Brown et al., 2005, Araki et al., 2017]. Indirect evidence are provided by geophysical methods (seismic tomography or magneto-tellurics) that show that domains characterized by seismic velocity anomalies or by low resistivities, which are explained by the presence of possibly overpressured fluids, overlap zones of nucleation of slow events. Besides, laboratory experiments carried out on oceanic crust rocks (gabbros, serpentinites) and numerical modeling further support the interplay between supra-hydrostatic p_f and slow earthquakes [Peacock, 2009, Katayama et al., 2012, Kitajima and Saffer, 2012, Beeler et al., 2013, Saffer and Wallace, 2015, Bernaudin and Gueydan, 2018, Condit et al., 2020, Dal Zilio and Gerya, 2022, Eberhard et al., 2022].

4.5.1. *Evidence in the geological record*

Tracking slow earthquake phenomena in the geological record is not easy, since rocks only exhibit frozen structures, for which strain rates are difficult to estimate. However, several studies contend that past slow slip events left tracks in surface-exhumed fault rocks (Table 8). Most of such studies pertain to ancient subduction interface-related slow events triggered or facilitated by near-lithostatic p_f. These studies are based on scenarii that are compatible with cyclic fracturing and fluid arrival in the fractured zones. One key issue in the slow-earthquake interpretation is the estimated duration of events. Based on silica diffusion from wall rock to quartz crak-seal veins found along a shear zone adjacent to a paleo-décollement in the Kodiak accretionary complex, Fisher and Brantley [2014] could estimate the time necessary to precipitate quartz for one crak-seal band as less than 10 days, which could correspond to the duration of some slow events in subduction zones. Similarly, based on a kinematic model of the growth of microscopic quartz bands following

Table 7. Examples of geophysical evidence for seismic swarms or seismic swarm-like sequences triggered or favored by abnormally high pore fluid pressures p_f in or around fault zones

Area and/or events	Evidence
Central and northern Japan (Matsushiro, Tohoku, Hida mountains, Hakone volcano)	Space–time evolution of seismicity fits with p_f diffusion laws[1],[2],[3]; pressurized fluid diffusion accounts for space–time evolution of seismicity along with Coulomb stress transfert and stress corrosion[4]; pressurized fluid diffusion and Coulomb stress transfert account for space–time evolution of seismicity[5]
Dobi graben seismic sequence, Afar rift, Djibouti	Space–time evolution of seismicity fits with p_f diffusion laws[6]
East African Rift, Uganda, Rwenzori region	Spatial overlap in the middle crust between intense volatile and CO_2 circulation and swarm hypocentral regions[7]
Central Europe (West Bohemia/Vogtland),	Space–time evolution of seismicity fits with p_f diffusion laws[8],[9], but static and dynamic Coulomb stress changes also play a role[10],[11],[12]; at about 9 km depth, $\lambda \sim 0.98$ ($p_f = 244$ MPa, that is 5 MPa below σ_v)[13]
Western Europe (Vosges mountains)	Space–time evolution of seismicity fits with p_f diffusion laws[14]
Western Alps (Ubaye region and vicinity)	Space–time evolution of seismicity fits with p_f diffusion laws[15],[16][17]; supra-hydrostatic p_f are necessary for reactivation of misoriented faults ($\lambda = 0.41$–0.51)[18]; time-space evolution of seismicity and development of excess p_f (between 35 and 55 MPa) explained by creep compaction[19]; space–time evolution of seismicity fits with p_f diffusion laws, but co-seismic stress transfer explains the seismicity close to the mainshock source[20]
Corinth rift	Space–time evolution of seismicity fits with p_f diffusion laws[21],[22]
Southern Italy, Mt Pollino region	Space–time evolution of seismicity fits with p_f diffusion laws[23]
Southern California (including Long Valley caldera)	Space–time evolution of seismicity fits with p_f diffusion laws[24],[25], possibly combined with episodic aseismic slip[26]

References: [1]Nur [1974], [2]Cappa et al. [2009], [3]Yoshida et al. [2016], [4]Aoyama et al. [2002], [5]Yukutake et al. [2011], [6]Noir et al. [1997], [7]Lindenfeld et al. [2012], [8]Parotidis et al. [2003], [9]Hainzl [2004], [10]Hainzl and Fischer [2002], [11]Fischer and Horálek [2005], [12]Fischer et al. [2014], [13]Vavryčuk [2002], [14]Audin et al. [2002], [15]Jenatton et al. [2007], [16]Godano et al. [2013], [17]Baques et al. [2021], [18]Leclère et al. [2012], [19]Leclère et al. [2013], [20]De Barros et al. [2019], [21]Duverger et al. [2015], [22]De Barros et al. [2020], [23]De Matteis et al. [2021], [24]Prejean et al. [2003], [25]Shelly et al. [2016], [26]Vidale and Shearer [2006].

cyclical pore fluid ingression in crack-seal veins from the Shimanto accretionary prism, Ujiie et al. [2018] could estimate the minimum duration of precipitation between two successive fluid pulses as less than 5 years. Such a duration is too low for standard earthquake rupture, but could correspond to episodic tremor and slip. Overall, the recognition of slow earthquakes in the geological record is still speculative, but quantification of duration of various inter-seismic or co-seismic phenomena such as mineral precipitation could validate the inferred geological signature of slow events.

Table 8. Examples of geological or geophysical evidence for present-day or past slow earthquakes triggered or favored by abnormally high pore fluid pressures p_f in or around fault zones

Setting	Area, structure, unit	Evidence
Present-day events along plate interfaces, subduction zones	Cascadia	Seismic imaging and seismic wave analyses suggest that p_f is near-lithostatic in a LVL inside which SSEs or ETSs nucleate[1],[2],[3],[4]; supra-hydrostatic p_f inferred in anisotropically permeable foliation parallel to the plate interface explains NVT distribution[5]; 3-D seismic tomography and magneto-tellurics show that LFEs nucleate in a landward dipping region characterized by a high Poisson ratio and by a high electrical conductivity; the region is interpreted as saturated by fluids trapped at near-lithostatic p_f[6]; variations in seismic velocities in the LVL after ETSs likely reflect p_f fluctuations[7]
	Middle America trench	Episodic fluid flow pulses measured in ODP boreholes correlate with seismic tremor in the frontal part of the plate interface and could reflect expulsion of transiently overpressured fluids[8]; SSEs nucleate in an ultra-slow velocity layer inside which fluids may be overpressured[9]; LFE occurrence during a SSE is interpreted to result from a p_f fluctuation having migrated updip along the subduction interface[10]
	NE Japan (Japan trench)	In the upper part of the downgoing Pacific, between 60 and 80 km depth, a zone of high V_P/V_S is accounted for by high p_f[11]
	SW Japan (Nankai subduction zone)	NVDT possibly linked with high p_f[12]; LFT suppressed where p_f is low[13]; slow slip is located in a high reflectivity and high Poisson ratio portion of the subducting oceanic crust[14]; NVT are located in a portion of the subducting oceanic crust characterized by V_P and V_S anomalies related to high p_f[15],[16]; SSE occur in a portion of the subducting slab characterized by seismic velocity anomalies likely caused by high p_f[17]; slow seismic slip in the shallow parts of the subduction interface is characterized by waves rich in high-frequency components, suggesting p_f-controlled tensile fractures[18]; p_f fluctuations measured in IODP boreholes correlate with SSEs in the shallow parts of the subduction interface[19],[20]

(continued on next page)

Table 8. (continued)

Setting	Area, structure, unit	Evidence
	New Zealand (Hikurangi margin)	Deep SSEs occur in a zone characterized by a high P wave attenuation and by a high V_P/V_S ratio, suggesting high p_f[21]; anomalously-shallow slow slip events occur in a low V_P zone where p_f is supposed to be supra-hydrostatic ($\lambda^* = 0.87$)[22]; 3-D V_P and V_P/V_S tomography from 8 to 70 km depth along the subduction interface, where both large shallow SSEs and small deep SSEs were recorded, is interpreted as subducted sediment with high p_f[23]; OBS data show that tectonic stresses in the subducting slab change throughout SSE cycles, possibly as a consequence of p_f fluctuations in the vicinity of the plate interface[24],[25]; repeating SSEs occur in a zone below which high V_P/V_S values suggest high p_f[26]
Present-day events along plate boundary transform faults	San Andreas fault	NVT activity near Parfield following large earthquakes seem to be enhanced by static shear stress and Coulomb stress increases, but p_f fluctuations at depth (15–30 km) may also play a role[27]; NVT near Parkfield likely reflect shear failure on a critically stressed fault in the presence of near-lithostatic p_f[28]
Evidence in the geological record along subduction zone plate interfaces	Namibia (Damara belt)	Hydrothermal quartz veins preserved in ductilely deformed rocks attest for hydrofracturing caused by high p_f during LFEs and VLFEs in the plastic aseismic regime below the seismogenic zone[29]
	Cyclades (Cycladic blueschist unit, Syros)	Brittle deformation structures (shear fractures and veins) in eclogite lenses embedded in ductilely deformed blueschist are interpreted to result from SSEs triggered by high p_f[30]
	SW Japan (Triassic Tomuru blueschists)	Quartz-filled crack-seal shear and extension veins in subduction mélange formed by frictional sliding and tensile fracturing at near-lithostatic p_f at short reccurrence times (a few years, determined from kinetic modeling of quartz precipitation) are tentatively accounted for by episodic strain release during ETSs[31]
	New Zealand (Dun ophiolite, Livingstone Fault)	Field and microstructural observations suggest that chemical reactions involving serpentinite can promote rock hardening and generate in situ fluid over-pressure patches and brittle failure in the source region of deep tremor along the slab-mantle interface[32]

(continued on next page)

Table 8. (continued)

Setting	Area, structure, unit	Evidence
	Alaska (Kodiak accretionary complex)	Quartz vein microstructures and estimation of duration of local silica diffusion indicate that near-lithostatic p_f can produce crack seal bands in less than 10 days, which is similar to the duration of slow earthquakes[33]
	Northern Apennines (continental metasediments)	Syn-mylonitization quartz-carpholite dilational shear veins formed under HP metamorphic conditions as a result of high p_f are interpreted as a record of deep ETS events[34]
	Central Alps (Arosa zone)	Crack-seal veins formed under blueschist facies conditions concurrently with viscous flow as a result of near-lithostatic p_f; the low estimated values of differential stresses suggest that the veins formed during slow slip and tremor events[35]
	California (Franciscan complex eastern belt)	Opening increments of ~1 mm in blueschist-facies metasediments are interpreted as the result of transient near-lithostatic p_f during LFEs[36]

References: [1]Abers et al. [2009], [2]Audet et al. [2009], [3]Tauzin et al. [2017], [4]Audet and Schaeffer [2018], [5]Delph et al. [2018], [6]Calvert et al. [2020], [7]Gosselin et al. [2020], [8]Brown et al. [2005], [9]Song et al. [2009], [10]Frank et al. [2015], [11]Shelly et al. [2006b], [12]Obara [2002], [13]Seno and Yamasaki [2003], [14]Kodaira et al. [2004], [15]Shelly et al. [2006a], [16]Matsubara et al. [2009], [17]Kato et al. [2010], [18]Sugioka et al. [2012], [19]Araki et al. [2017], [20]Ariyoshi et al. [2021], [21]Wallace and Eberhart-Phillips [2013], [22]Bassett et al. [2014], [23]Eberhart-Phillips and Bannister [2015], [24]Shaddox and Schwartz [2019], [25]Warren-Smith et al. [2019], [26]Yarce et al. [2021], [27]Nadeau and Guilhem [2009], [28]Thomas et al. [2009], [29]Fagereng et al. [2018], [30]Behr et al. [2018], [31]Ujiie et al. [2018], [32]Tarling et al. [2019], [33]Fisher and Brantley [2014], [34]Giuntoli and Viola [2021], [35]Condit and French [2022], [36]Schmidt and Platt [2022].

LVL: low-velocity layer. SSE: slow-slip event. ETS: episodic tremor and slip. NVT: non-volcanic tremor. 3-D: three-dimensional. LFE: low-frequency earthquake. NVDT: non-volcanic deep tremor. ODP: Ocean Drilling Program. LFT: low-frequency tremor. OBS: ocean-bottom seismometer. VLFE: very low frequency earthquake. HP: high pressure.

4.6. *Fluids and man-made earthquakes*

Several man-made earthquakes show that fluids can trigger seismic ruptures. One emblematic piece of evidence for this triggering role is the earthquake activity that occurred in Colorado following waste water disposal at depth [Healy et al., 1968]. Experimental water injection at depth at Rangely [Colorado, Raleigh et al., 1976] confirmed than fluids could trigger earthquakes. Since then, the artifical triggering of earthquakes has been ascertained in a large variety of human activities: hydrocarbon extraction [Wiprut and Zoback, 2000, Amos et al., 2014, Bourne et al., 2014, Van Wees et al., 2014], dam reservoir impoundment [Rastogi et al., 1997, Gupta, 2002, McGarr et al., 2002, Zhang et al., 2019], industrial waste water repository [Horton, 2012, Yeck et al., 2016], carbon dioxide storage projects [Zoback and Gorelick, 2012], and water injection in deep boreholes to produce geothermal energy [Deichmann and Giardini, 2009, Terakawa et al., 2012, McGarr et al., 2015]. Fluid-injection-experiments at the KTB borehole in Germany have shown that even small pressure variations (<1 MPa) could trigger numerous microearthquakes at a depth of 9 km [Zoback and Harjes, 1997]. In most case studies, the p_f build-up in the vicinity of critically loaded faults is responsible for failure. However, abnormally high p_f may also act indirectly by triggering aseismic slip which in turn leads to an earthquake [Wei et al., 2015]. Lastly, stress perturbations by Coulomb stress transfer can also contribute to man-induced seismic ruptures [De Matteis et al., 2024].

4.7. *Conclusions*

The interactions between fluids and seismic ruptures in the brittle crust or in subducting slabs are more and more recognized or suspected (Tables 5–8). The role of overpressured fluids in the triggering or propagation of small-magnitude events such as aftershocks, swarms and, to a lesser extent, slow earthquakes, seems to be well established. Regarding large-magnitude events, the role of excess pore fluid pressures is more difficult to ascertain. However, a large body of evidence suggests that seismic ruptures, especially those along plate interfaces in subduction zones, take place in crustal volumes where seismic tomography indicates body wave velocity anomalies that are interpreted as the consequence of the presence of overpressured fluids. The present review of literature further shows that abnormally high pore fluid pressures may not be the only mechanism. Indeed, stress perturbations can act in concert with abnormally high p_f and the inferred decrease of σ_n.

5. Conclusions

A review of the literature shows that fluids physically interact everywhere and at all scales with deformation in the brittle crust and in subducting slabs. Since they are more permeable than most intact rocks, fractures, faults and shear zones in the brittle or brittle-ductile crust and in the subducting slabs appear as efficient paths for fluid circulation. Provided that impervious seals develop transiently or permanently, fluids can accumulate and their pressure can increase. Where faults are critically stressed, only a minor overpressure value (a few MPa above the hydrostatic pressure) can trigger or favor rupture or displacement. Where faults are not critically stressed, for instance where they are severely misoriented with respect to the active stress tensor, larger excess p_f values are needed for reactivation. Fluid overpressures can be estimated by using chemical data or fluid inclusion data in exhumed rocks. Estimated values are as follows: 25–135 MPa at seismogenic depths [*ca.* 5 to 10 km, Shimanto paleo-accretionary prism, Raimbourg et al., 2022, Kodiak paleo-accretionary prism, Vrolijk, 1987], 50–150 MPa at 8–9 km [Apennines, Mullis, 1988], 110 MPa at *ca.* 20 km [Central Alps, Berger and Herwegh, 2019], 200–350 MPa at 8–10 km or deeper [Val d'Or district, Canada, Robert et al., 1995], 100–350 MPa at 30–70 km in an exhumed subducted lithosphere [Viete et al., 2018].

The influence of abnormally high p_f is of utmost importance in the triggering or in the propagation of seismic ruptures. The p_f effect appears to be common in small to moderate magnitude ($M < 5 \sim 6$) events such as aftershocks or swarm sequences. The role of high p_f is less obvious for large magnitude ($M > 6$ or higher) events. However, the precursor mechanisms preceding large magnitude events may be partly controlled by p_f build-up. Future researches will concentrate on this aspect of the seismic cycle. In particular, a critical issue is to try to determine whether a p_f increase is the triggering (causal) mechanism for a seismic rupture propagation or is a consequence of a propagating rupture triggered by a mechanism that would not be related to p_f. In their spatio-temporal monitoring of V_P and V_S variations during the 1997 Umbria-Marche sequence, central Italy (Table 5), Chiarabba et al. [2009a] suggest that the p_f propagation precedes the seismic ruptures. A similar conclusion is reached by Yoshida et al. [2023] in their study of a swarm sequence resulting in a M_w 6.2 event in NE Japan. Besides, the *in-situ* experiments of Guglielmi et al. [2015] and Cappa et al. [2022] show that a p_f increase triggers aseismic slip that eventually turns into a seismic displacement. From their field study of intermediate-depth earthquakes frozen in an ancient oceanic crust, John and Schenk [2006] conclude that seismic rupture was not preceded but rather accompanied and followed by fluid ingression in the hypocentral volume (Table 6). Further experimental or *in situ* works along with detailed geological or geophysical analyses are obviously needed before the complex interrelationships between p_f variation and inception or propagation of brittle fracture or slip along faults can be fully understood.

High p_f values also play a role in the triggering or maintenance of slow slip earthquakes and related phenomena along several subduction interfaces or along transform faults. Since these transient phenomena can in turn influence or control large-magnitude seismic ruptures, a careful analysis or monitoring of p_f build-up is an important direction of future research. The precursory results of Brown et al. [2005], Mikada et al. [2006], Fulton and Brodsky [2016] or Ariyoshi et al. [2021] are examples of such a promising monitoring.

Declaration of interests

The authors do not work for, advise, own shares in, or receive funds from any organization that could benefit from this article, and have declared no affiliations other than their research organizations.

References

Abers, G. A. (2009). Slip on shallow-dipping normal faults. *Geology*, 37, 767–768.

Abers, G. A., MacKenzie, L. S., Rondenay, S., Zhang, Z., Wech, A. G., and Creager, K. C. (2009). Imaging the source region of Cascadia tremor and intermediate-depth earthquakes. *Geology*, 37, 1119–1122.

Amos, C. B., Audet, P., Hammond, W. C., Bürgmann, R., Johanson, I. A., and Blewitt, G. (2014). Uplift and seismicity driven by groundwater depletion in central California. *Nature*, 509, 483–486.

Anderson, O. L. and Grew, P. C. (1977). Stress corrosion theory of crack propagation with applications to geophysics. *Rev. Geophys. Space Phys.*, 15, 77–104.

Angiboust, S., Kirsch, J., Oncken, O., Glodny, J., Monié, P., and Rybacki, E. (2015). Probing the transition between seismically coupled and decoupled segments along an ancient subduction interface. *Geochem. Geophys. Geosyst.*, 16, 1905–1922.

Angiboust, S. and Raimondo, T. (2022). Permeability of subducted oceanic crust revealed by eclogite-facies vugs. *Geology*, 50, 964–968.

Antonioli, A., Piccinini, D., Chiaraluce, L., and Cocco, M. (2005). Fluid flow and seismicity pattern: Evidence from the 1997 Umbria-Marche (central Italy) seismic sequence. *Geophys. Res. Lett.*, 32, article no. L10311.

Aoyama, H., Takeo, M., and Ide, S. (2002). Evolution mechanisms of an earthquake swarm under the Hida Mountains, central Japan, in 1998. *J. Geophys. Res.*, 107, article no. 2174.

Araki, E., Saffer, D. M., Kopf, A. J., Wallace, L. M., Kimura, T., Machida, Y., Ide, S., Davis, E., and IODP Expedition 365 shipboard scientists (2017). Recurring and triggered slow-slip events near the trench at the Nankai Trough subduction megathrust. *Science*, 356, 1157–1160.

Ariyoshi, K., Kimura, T., Miyazawa, Y., Varlamov, S., Iinuma, T., Nagano, A., Gomberg, J., Araki, E., Miyama, T., Sueki, K., Yada, S., Hori, T., Takahashi, N., and Kodaira, S. (2021). Precise monitoring of pore pressure at boreholes around Nankai Trough toward early detecting crustal deformation. *Front. Earth Sci.*, 9, article no. 717696.

Atkinson, B. K. (1984). Subcritical crack growth in geological materials. *J. Geophys. Res.*, 89, 4077–4114.

Audet, P., Bostock, M. G., Christensen, N. I., and Peacock, S. M. (2009). Seismic evidence for overpressured subducted oceanic crust and megathrust fault sealing. *Nature*, 457, 76–78.

Audet, P. and Schaeffer, A. J. (2018). Fluid pressure and shear zone development over the locked to slow slip region in Cascadia. *Sci. Adv.*, 4, article no. eaar2982.

Audet, P. and Schwartz, S. Y. (2013). Hydrologic control of forearc strength and seismicity in the Costa Rican subduction zone. *Nat. Geosci.*, 6, 852–855.

Audin, L., Avouac, J. P., Flouzat, M., and Plantet, J. L. (2002). Fluid-driven seismicity in a stable tectonic context: The Remiremont fault zone, Vosges, France. *Geophys. Res. Lett.*, 29, article no. 1091.

Axen, G. J. (1992). Pore pressure, stress increase, and fault weakening in low-angle normal faulting. *J. Geophys. Res.*, 97, 8979–8991.

Axen, G. J., Bartley, J. M., and Selverstone, J. (1995). Structural expression of a rolling hinge in the footwall of the Brenner Line normal fault, eastern Alps. *Tectonics*, 14, 1380–1392.

Axen, G. J., Selverstone, J., and Wawrzyniec, T. (2001). High-temperature embrittlement of extensional Alpine mylonite zones in the midcrustal ductile-brittle transition. *J. Geophys. Res.*, 106, 4337–4348.

Badertscher, N. P., Beaudouin, G., Therrien, R., and Burkhard, M. (2002). Glarus overthrust: A major pathway for the escape of fluids out of the Alpine orogen. *Geology*, 30, 875–878.

Badertscher, N. P. and Burkhard, M. (2000). Brittle-ductile deformation in the Glarus thrust Lochseiten (LK) calc-mylonite. *Terra Nova*, 12, 281–288.

Bangs, N. L., Shipley, T. H., Gulick, S. P., Moore, G. F., Kuromoto, S., and Nakamura, Y. (2004). Evolution of the Nankai Trough décollement from the trench into the seismogenic zone: Inferences from three-dimensional seismic reflection imaging. *Geology*, 32, 273–276.

Bangs, N. L., Westbrook, G. K., Ladd, J., and Buhl, P. (1990). Seismic velocities from the Barbados Ridge complex: Indicators of high pore fluid pressures in an accretionary complex. *J. Geophys. Res.*, 95, 8767–8782.

Baques, M., De Barros, L., Duverger, C., Jomard, H., Godano, M., Courboulex, F., and Larroque, C. (2021). Seismic activity in the Ubaye Region (French Alps): a specific behavior highlighted by mainshocks and swarm sequences. *C. R. Géosci.*, 353, 535–559.

Barr, T. D. and Dahlen, F. A. (1990). Constraints on friction and stress in the Taiwan fold-and-thrust belt from heat flow and geochronology. *Geology*, 18, 111–115.

Bassett, D., Sutherland, R., and Henrys, S. (2014). Slow wavespeeds and fluid overpressure in a region of shallow geodetic locking and slow slip, Hikurangi subduction margin, New Zealand. *Earth Planet. Sci. Lett.*, 389, 1–13.

Beeler, N. M., Thomas, A., Bürgmann, R., and Shelly, D. (2013). Inferring fault rheology from low-frequency earthquakes on the San Andreas. *J. Geophys. Res.*, 118, 5976–5990.

Behr, W. M., Kotowski, A. J., and Ashley, K. T. (2018). Dehydration-induced rheological heterogeneity and the deep tremor source in warm subduction zones. *Geology*, 46, 475–478.

Behrmann, J. H. (1991). Conditions for hydrofracture and the fluid permeability of accretionary wedges. *Earth Planet. Sci. Lett.*, 107, 550–558.

Berger, A. and Herwegh, M. (2019). Cockade structures as a paleo-earthquake proxy in upper crustal hydrothermal systems. *Sci. Rep.*, 9, article no. 9209.

Bernaudin, M. and Gueydan, F. (2018). Episodic tremor and slip explained by fluid-enhanced microfracturing and sealing. *Geophys. Res. Lett.*, 45, 3471–3480.

Bettinelli, P., Avouac, J. P., Flouzat, M., Bollinger, L., Ramillien, G., Rajaure, S., and Sapkota, S. (2008). Seasonal variations of seismicity and geodetic strain in the Himalaya induced by surface hydrology. *Earth Planet. Sci. Lett.*, 266, 332–344.

Blanpied, M. L., Lockner, D. A., and Byerlee, J. D. (1992). An earthquake mechanism based on rapid sealing of faults. *Nature*, 358, 574–576.

Bloch, W., John, T., Kummerow, J., Salazar, P., Krüger, O. S., and Shapiro, S. A. (2018). Watching dehydration: Seismic indication for transient fluid pathways in the oceanic mantle of the subducting Nazca slab. *Geochem. Geophys. Geosyst.*, 19, 3189–3207.

Boncio, P. and Bracone, V. (2009). Active stress from earthquake focal mechanisms along the Padan-Adriatic side of the Northern Apennines (Italy), with considerations on stress magnitudes and pore-fluid pressures. *Tectonophysics*, 476, 180–194.

Bosl, W. J. and Nur, A. (2002). Aftershocks and pore fluid diffusion following the 1992 Landers earthquake. *J. Geophys. Res.*, 107, article no. 2366.

Boullier, A. M. (2011). Fault-zone geology: lessons from drilling through the Nojima and Chelungpu faults. *Geol. Soc. London Spec. Publ.*, 359, 17–37.

Boullier, A. M., Yeh, E. C., Boutareaud, S., Song, S. R., and Tsai, C. H. (2009). Microscale anatomy of the 1999 Chi-Chi earthquake fault zone. *Geochem. Geophys. Geosyst.*, 10, article no. Q03016.

Bourne, S. J., Oates, S. J., van Elk, J., and Doornhof, D. (2014). A seismological model for earthquakes induced by fluid extraction from a subsurface reservoir. *J. Geophys. Res.*, 119, 8991–9015.

Boutareaud, S., Hirose, T., Andréani, M., Pec, M., Calugaru, D. G., Boullier, A. M., and Doan, M. L. (2012). On the role of phyllosilicates on fault lubrication: Insight from micro- and nano-structural investigations on talc friction experiments. *J. Geophys. Res.*, 117, B08408.

Boutareaud, S., Wibberley, C. A., Fabbri, O., and Shimamoto, T. (2008). Permeability structure and coseismic thermal pressurization on fault branches: Insights from the Usukidani Fault, Japan. *Geol. Soc. London Spec. Publ.*, 299, 341–361.

Brantut, N., Heap, M. J., Meredith, P. G., and Baud, P. (2013). Time-dependent cracking and brittle creep in crustal rocks: A review. *J. Struct. Geol.*, 52, 17–43.

Brantut, N., Schubnel, A., Corvisier, J., and Sarout, J. (2010). Thermochemical pressurization of faults during coseismic slip. *J. Geophys. Res.*, 115, article no. B05314.

Brantut, N., Schubnel, A., Rouzaud, J. N., Brunet, F., and Shimamoto, T. (2008). High-velocity frictional properties of a clay-bearing fault gouge and implications for earthquake mechanics. *J. Geophys. Res.*, 113, article no. B10401.

Brown, K. M., Kopf, A., Underwood, M. B., and Weinberger, J. L. (2003). Compositional and fluid pressure controls on the state of stress on the Nankai subduction thrust: A weak plate boundary. *Earth Planet. Sci. Lett.*, 214, 589–603.

Brown, K. M., Tryon, M. D., DeShon, H. R., Dorman, L. M., and Schwartz, S. Y. (2005). Correlated transient fluid pulsing and seismic tremor in the Costa Rica subduction zone. *Earth Planet. Sci. Lett.*, 238, 189–203.

Burkhard, M., Kerrich, R., Maas, R., and Fyfe, W. S. (1992). Stable and Sr-isotope evidence for fluid advection during thrusting of the Glarus nappe (Swiss Alps). *Contrib. Mineral. Petrol.*, 112, 293–311.

Byerlee, J. (1978). Friction of rocks. *Pure Appl. Geophys.*, 116, 615–626.

Byerlee, J. (1990). Friction, overpressure and fault normal compression. *Geophys. Res. Lett.*, 17, 2109–2112.

Byerlee, J. (1993). Model for episodic flow of high-pressure water in fault zones before earthquakes. *Geology*, 21, 303–306.

Byrne, T. and Fisher, D. (1990). Evidence for a weak and overpressured decollement beneath sediment-dominated accretionary prisms. *J. Geophys. Res.*, 95, 9081–9097.

Calderoni, G., Di Giovambattista, R., Burrato, P., and Ventura, G. (2009). A seismic sequence from Northern Apennines (Italy) provides new insight on the role of fluids in the active tectonics of accretionary wedges. *Earth Planet. Sci. Lett.*, 281, 99–109.

Calvert, A. J., Bostock, M. G., Savard, G., and Unsworth, M. J. (2020). Cascadia low frequency earthquakes at the base of an overpressured subduction shear zone. *Nat. Commun.*, 11, article no. 3874.

Cappa, F., Guglielmi, Y., Nussbaum, C., De Barros, L., and Birkholzer, J. (2022). Fluid migration in low-permeability faults driven by decoupling of fault slip and opening. *Nat. Geosci.*, 15, 747–751.

Cappa, F., Rutqvist, J., and Yamamoto, K. (2009). Modeling crustal deformation and rupture processes related to upwelling of deep CO_2-rich fluids during the 1965–1967 Matsushiro earthquake swarm in Japan. *J. Geophys. Res.*, 114, article no. B10304.

Carpenter, B. M., Marone, C., and Saffer, D. M. (2011). Weakness of the San Andreas Fault revealed by samples from the active fault zone. *Nat. Geosci.*, 4, 251–254.

Castelain, T., McCaig, A. M., and Cliff, R. A. (2014). Fluid evolution in an oceanic core complex: A fluid inclusion study from IODP hole U1309 D—Atlantis Massif, 30° N, Mid-Atlantic Ridge. *Geochem. Geophys. Geosyst.*, 15, 1193–1214.

Cattin, R. and Avouac, J. P. (2000). Modeling mountain building and the seismic cycle in the Himalaya of Nepal. *J. Geophys. Res.*, 105, 13389–13407.

Chapple, W. M. (1978). Mechanics of thin-skinned fold-and-thrust belts. *Geol. Soc. Am. Bull.*, 89, 1189–1198.

Chen, X., Elwood Madden, A. S., and Reches, Z. (2017). The frictional strength of talc gouge in high-velocity shear experiments. *J. Geophys. Res.*, 122, 3661–3676.

Chiarabba, C., De Gori, P., and Boschi, E. (2009a). Pore-pressure migration along a normal-fault system resolved by time-repeated seismic tomography. *Geology*, 37, 67–70.

Chiarabba, C., Piccinini, D., and De Gori, P. (2009b). Velocity and attenuation tomography of the Umbria Marche 1997 fault system: Evidence of a fluid-governed seismic sequence. *Tectonophysics*, 476, 73–84.

Chiodini, G., Caliro, S., Cardellini, C., Frondini, F., Inguaggiato, S., and Matteucci, F. (2011). Geochemical evidence for and characterization of CO_2 rich gas sources in the epicentral area of the Abruzzo 2009 earthquakes. *Earth Planet. Sci. Lett.*, 304, 389–398.

Chiodini, G., Cardellini, C., Amato, A., Boschi, E., Caliro, S., and Frondini, F. (2004). Carbon dioxide Earth degassing and seismogenesis in central and southern Italy. *Geophys. Res. Lett.*, 31, article no. L07615.

Clemenzi, L., Storti, F., Balsamo, F., Molli, G., Ellam, R., Muchez, P., and Swennen, R. (2015). Fluid pressure cycles, variations in permeability, and weakening mechanisms along low-angle normal faults: The Tellaro detachment, Italy. *Geol. Soc. Am. Bull.*, 127, 1689–1710.

Cobbold, P. R., Durand, S., and Mourgues, R. (2001). Sandbox modelling of thrust wedges with fluid-assisted detachments. *Tectonophysics*, 334, 245–258.

Cochrane, G. R., Moore, J. C., and Lee, H. J. (1996). Sediment pore-fluid overpressuring and its effect on deformation at the toe of the Cascadia accretionary prism from seismic velocities. In *Subduction: Top to Bottom*, pages 57–64. John Wiley and Sons, Hoboken, NJ.

Cochrane, G. R., Moore, J. C., MacKay, M. E., and Moore, G. F. (1994). Velocity and inferred porosity model of the Oregon accretionary prism from multichannel seismic reflection data: Implications on sediment dewatering and overpressure. *J. Geophys. Res.*, 99, 7033–7043.

Collettini, C. (2011). The mechanical paradox of low-angle normal faults: Current understanding and open questions. *Tectonophysics*, 510, 253–268.

Collettini, C., Cardellini, C., Chiodini, G., De Paola, N., Holdsworth, R. E., and Smith, S. A. F. (2008). Fault weakening due to CO_2 degassing in the Northern Apennines: short- and long-term processes. *Geol. Soc. London Spec. Publ.*, 299, 175–194.

Collettini, C., De Paola, N., and Faulkner, D. R. (2009a). Insights on the geometry and mechanics of the Umbria-Marche earthquakes (Central Italy) from the integration of field and laboratory data. *Tectonophysics*, 476, 99–109.

Collettini, C. and Holdsworth, R. E. (2004). Fault zone weakening and character of slip along low-angle normal faults: Insights from the Zuccale fault, Elba, Italy. *J. Geol. Soc.*, 161, 1039–1051.

Collettini, C., Viti, C., Smith, S. A., and Holdsworth, R. E. (2009b). Development of interconnected talc networks and weakening of continental low-angle normal faults. *Geology*, 37, 567–570.

Condit, C. B. and French, M. E. (2022). Geologic evidence of lithostatic pore fluid pressures at the base of the subduction seismogenic zone. *Geophys. Res. Lett.*, 49, article no. e2022GL098862.

Condit, C. B., Guevara, V. E., Delph, J. R., and French, M. E. (2020). Slab dehydration in warm subduction zones at depths of episodic slip and tremor. *Earth Planet. Sci. Lett.*, 552, article no. 116601.

Cosgrove, J. W. (1995). The expression of hydraulic fracturing in rocks and sediments. *Geol. Soc. London Spec. Publ.*, 92, 187–187.

Costa, E. and Vendeville, B. C. (2002). Experimental insights on the geometry and kinematics of fold-and-thrust belts above weak, viscous evaporitic décollement. *J. Struct. Geol.*, 24, 1729–1739.

Cox, S. F. (1995). Faulting processes at high fluid pressures: an example of fault valve behavior from the Wattle Gully Fault, Victoria, Australia. *J. Geophys. Res.*, 100, 12841–12859.

Cox, S. F. (2010). The application of failure mode diagrams for exploring the roles of fluid pressure and stress states in controlling styles of fracture-controlled permeability enhancement in faults and shear zones. *Geofluids*, 10, 217–233.

Cox, S. F. and Ruming, K. (2004). The St Ives mesothermal gold system, Western Australia-a case of golden aftershocks? *J. Struct. Geol.*, 26, 1109–1125.

Crespo-Blanc, A., Masson, H., Sharp, Z., Cosca, M., and Hunziker, J. (1995). A stable and $^{40}Ar/^{39}Ar$ isotope study of a major thrust in the Helvetic nappes (Swiss Alps): evidence for fluid flow and constraints on nappe kinematics. *Geol. Soc. Am. Bull.*, 107, 1129–1144.

Dal Zilio, L. and Gerya, T. (2022). Subduction earthquake cycles controlled by episodic fluid pressure cycling. *Lithos*, 426, article no. 106800.

Davis, D., Suppe, J., and Dahlen, F. A. (1983). Mechanics of fold-and-thrust belts and accretionary wedges. *J. Geophys. Res.*, 88, 1153–1172.

Davis, D. M. and Engelder, T. (1985). The role of salt in fold-and-thrust belts. *Tectonophysics*, 119, 67–88.

Davis, E. E. and Villinger, H. W. (2006). Transient formation fluid pressures and temperatures in the Costa Rica forearc prism and subducting oceanic basement: CORK monitoring at ODP Sites 1253 and 1255. *Earth Planet. Sci. Lett.*, 245, 232–244.

De Barros, L., Baques, M., Godano, M., Helmstetter, A., Deschamps, A., Larroque, C., and Courboulex, F. (2019). Fluidinduced swarms and coseismic stress transfer: A dual process highlighted in the aftershock sequence of the 7 April 2014 earthquake (Ml 4.8, Ubaye, France). *J. Geophys. Res.*, 124, 3918–3932.

De Barros, L., Cappa, F., Deschamps, A., and Dublanchet, P. (2020). Imbricated aseismic slip and fluid diffusion drive a seismic swarm in the Corinth Gulf, Greece. *Geophys. Res. Lett.*, 47, article no. e2020GL087142.

De Matteis, R., Convertito, V., Napolitano, F., Amoroso, O., Terakawa, T., and Capuano, P. (2021). Pore fluid pressure imaging of the Mt. Pollino region (southern Italy) from earthquake focal mechanisms. *Geophys. Res. Lett.*, 48, article no. e2021GL094552.

De Matteis, R., Massa, B., Adinolfi, G. M., Amoroso, O., Terakawa, T., and Convertito, V. (2024). Pore fluid pressure in St. Gallen geothermal field (Switzerland) based on earthquake focal mechanisms. *Geophys. Res. Lett.*, 51, article no. e2023GL105127.

Deichmann, N. (1992). Structural and rheological implications of lower-crustal earthquakes below northern Switzerland. *Phys. Earth Planet. Inter.*, 69, 270–280.

Deichmann, N. and Giardini, D. (2009). Earthquakes induced by the stimulation of an enhanced geothermal system below Basel (Switzerland). *Seismol. Res. Lett.*, 80, 784–798.

Delph, J. R., Levander, A., and Niu, F. (2018). Fluid controls on the heterogeneous seismic characteristics of the Cascadia margin. *Geophys. Res. Lett.*, 45, 11021–11029.

Deville, E. (2021). Structure of the tectonic front of the Western Alps: Control of fluid pressure and halite occurrence on the decollement processes. *Tectonics*, 40, article no. e2020TC006591.

Di Luccio, F., Palano, M., Chiodini, G., et al. (2022). Geodynamics, geophysical and geochemical observations, and the role of CO_2 degassing in the Apennines. *Earth Sci. Rev.*, 234, article no. 104236.

Di Luccio, F., Ventura, G., Di Giovambattista, R., Piscini, A., and Cinti, F. R. (2010). Normal faults and thrusts reactivated by deep fluids: The 6 April 2009 Mw 6.3 L'Aquila earthquake, central Italy. *J. Geophys. Res.*, 115, article no. B06315.

Duverger, C., Godano, M., Bernard, P., Lyon-Caen, H., and Lambotte, S. (2015). The 2003–2004 seismic swarm in the western Corinth rift: Evidence for a multiscale pore pressure diffusion process along a permeable fault system. *Geophys. Res. Lett.*, 42, 7374–7382.

Eberhard, L., Thielmann, M., Eichheimer, P., Néri, A., Suzuki, A., Ohl, M., Fujita, W., Uesugi, K., Nakamura, M., Golabek, G. J., and Frost, D. J. (2022). A new method for determining fluid flux at high pressures applied to the dehydration of serpentinites. *Geochem. Geophys. Geosyst.*, 23, article no. e2021GC010062.

Eberhart-Phillips, D. and Bannister, S. (2015). 3-D imaging of the northern Hikurangi subduction zone, New Zealand: variations in subducted sediment, slab fluids and slow slip. *Geophys. J. Int.*, 201, 838–855.

Eberhart-Phillips, D. and Michael, A. J. (1993). Three-dimensional velocity structure, seismicity, and fault structure in the Parkfield Region, Central California. *J. Geophys. Res.*, 98, 15737–15758.

Escartin, J., Mével, C., MacLeod, C. J., and McCaig, A. M. (2003). Constraints on deformation conditions and the origin of oceanic detachments: The Mid-Atlantic Ridge core complex at 15° 45′ N. *Geochem. Geophys. Geosyst.*, 4, article no. 1067.

Evans, J. P. and Chester, F. M. (1995). Fluid-rock interaction in faults of the San Andreas system: Inferences from San Gabriel fault rock geochemistry and microstructures. *J. Geophys. Res.*, 100, 13007–13020.

Fagereng, Å., Diener, J. F., Meneghini, F., Harris, C., and Kvadsheim, A. (2018). Quartz vein formation by local dehydration embrittlement along the deep, tremorgenic subduction thrust interface. *Geology*, 46, 67–70.

Fagereng, Å., Remitti, F., and Sibson, R. H. (2010). Shear veins observed within anisotropic fabric at high angles to the maximum compressive stress. *Nat. Geosci.*, 3, 482–485.

Fagereng, Å., Remitti, F., and Sibson, R. H. (2011). Incrementally developed slickenfibers—Geological record of repeating low stress-drop seismic events? *Tectonophysics*, 510, 381–386.

Faleiros, F. M., da Cruz Campanha, G. A., da Silveira Bello, R. M., and Fuzikawa, K. (2007). Fault-valve action and vein development during strike-slip faulting: An example from the Ribeira Shear Zone, Southeastern Brazil. *Tectonophysics*, 438, 1–32.

Famin, V. and Nakashima, S. (2005). Hydrothermal fluid venting along a seismogenic detachment fault in the Moresby rift (Woodlark basin, Papua New Guinea). *Geochem. Geophys. Geosyst.*, 6, article no. Q12003.

Famin, V., Nakashima, S., Boullier, A. M., Fujimoto, K., and Hirono, T. (2008). Earthquakes produce carbon dioxide in crustal faults. *Earth Planet. Sci. Lett.*, 265, 487–497.

Famin, V., Raimbourg, H., Garcia, S., Bellahsen, N., Hamada, Y., Boullier, A. M., Fabbri, O., Michon, L., Uchide, T., Ricci, T., Hirono, T., and Kawabata, K. (2014). Stress rotations and the longterm weakness of the Median Tectonic Line and the RokkoAwaji Segment. *Tectonics*, 33, 1900–1919.

Faulkner, D. R., Mitchell, T. M., Healy, D., and Heap, M. J. (2006). Slip on weak' faults by the rotation of regional stress in the fracture damage zone. *Nature*, 444, 922–925.

Faulkner, D. R. and Rutter, E. H. (2001). Can the maintenance of overpressured fluids in large strike-slip fault zones explain their apparent weakness? *Geology*, 29, 503–506.

Ferri, F., Di Toro, G., Hirose, T., and Shimamoto, T. (2010). Evidence of thermal pressurization in highvelocity friction experiments on smectiterich gouges. *Terra Nova*, 22, 347–353.

Fischer, T. and Horálek, J. (2005). Slip-generated patterns of swarm microearthquakes from West Bohemia/Vogtland (central Europe): Evidence of their triggering mechanism? *J. Geophys. Res.*, 110, article no. B05S21.

Fischer, T., Horálek, J., Hrubcová, P., Vavryčuk, V., Bräuer, K., and Kämpf, H. (2014). Intra-continental earthquake swarms in West-Bohemia and Vogtland: a review. *Tectonophysics*, 611, 1–27.

Fisher, D. and Byrne, T. (1987). Structural evolution of underthrusted sediments, Kodiak Islands, Alaska. *Tectonics*, 6, 775–793.

Fisher, D. M. and Brantley, S. L. (2014). The role of silica redistribution in the evolution of slip instabilities along subduction interfaces: Constraints from the Kodiak accretionary complex, Alaska. *J. Struct. Geol.*, 69, 395–414.

Fisher, D. M., Brantley, S. L., Everett, M., and Dzvonik, J. (1995). Cyclic fluid flow through a regionally extensive fracture network within the Kodiak accretionary prism. *J. Geophys. Res.*, 100, 12881–12894.

Floyd, J. S., Mutter, J. C., Goodliffe, A. M., and Taylor, B. (2001). Evidence for fault weakness and fluid flow within an active low-angle normal fault. *Nature*, 411, 779–783.

Frank, W. B., Shapiro, N. M., Husker, A. L., Kostoglodov, V., Bhat, H. S., and Campillo, M. (2015). Along-fault pore-pressure evolution during a slow-slip event in Guerrero, Mexico. *Earth Planet. Sci. Lett.*, 413, 135–143.

French, M. E. and Morgan, J. K. (2020). Pore fluid pressures and strength contrasts maintain frontal fault activity, northern Hikurangi margin, New Zealand. *Geophys. Res. Lett.*, 47, article no. e2020GL089209.

Frohlich, C. (2006). *Deep Earthquakes*. Cambridge University Press, Cambridge.

Früh-Green, G. L., Weissert, H., and Bernoulli, D. (1990). A multiple fluid history recorded in Alpine ophiolites. *J. Geol. Soc.*, 147, 959–970.

Fulton, P. M. and Brodsky, E. E. (2016). In situ observations of earthquake-driven fluid pulses within the Japan Trench plate boundary fault zone. *Geology*, 44, 851–854.

Fulton, P. M. and Saffer, D. M. (2009). Potential role of mantle-derived fluids in weakening the San Andreas Fault. *J. Geophys. Res.*, 114, article no. B07408.

Fulton, P. M., Saffer, D. M., and Bekins, B. A. (2009). A critical evaluation of crustal dehydration as the cause of an overpressured and weak San Andreas Fault. *Earth Planet. Sci. Lett.*, 284, 447–454.

Gardonio, B., Jolivet, R., Calais, E., and Leclère, H. (2018). The April 2017 Mw 6.5 Botswana earthquake: An intraplate event triggered by deep fluids. *Geophys. Res. Lett.*, 45, 8886–8896.

Giuntoli, F., Menegon, L., Siron, G., Cognigni, F., Leroux, H., Compagnoni, R., Rossi, M., and Vitale Brovarone, A. (2024). Methane-hydrogen-rich fluid migration may trigger seismic failure in subduction zones at forearc depths. *Nat. Commun.*, 15, article no. 480.

Giuntoli, F. and Viola, G. (2021). Cyclic brittle-ductile oscillations recorded in exhumed high-pressure continental units: A record of deep episodic tremor and slow slip events in the northern Apennines. *Geochem. Geophys. Geosyst.*, 22, 1–27.

Godano, M., Larroque, C., Bertrand, E., Courboulex, F., Deschamps, A., Salichon, J., Blaud-Guerry, C., Fourteau, L., Charléty, J., and Deshayes, P. (2013). The October–November 2010 earthquake swarm near Sampeyre (Piedmont region, Italy): A complex multicluster sequence. *Tectonophysics*, 608, 97–111.

Gosselin, J. M., Audet, P., Estève, C., McLellan, M., Mosher, S. G., and Schaeffer, A. J. (2020). Seismic evidence for megathrust fault-valve behavior during episodic tremor and slip. *Sci. Adv.*, 6, article no. eaay5174.

Gueydan, F., Leroy, Y. M., Jolivet, L., and Agard, P. (2003). Analysis of continental midcrustal strain localization induced by microfracturing and reactionsoftening. *J. Geophys. Res.*, 108, article no. 2064.

Guglielmi, Y., Cappa, F., Avouac, J. P., Henry, P., and Elsworth, D. (2015). Seismicity triggered by fluid injection-induced aseismic slip. *Science*, 348, 1224–1226.

Gupta, H. K. (2002). A review of recent studies of triggered earthquakes by artificial water reservoirs with special emphasis on earthquakes in Koyna, India. *Earth Sci. Rev.*, 58, 279–310.

Gutiérrez-Aguilar, F., Hernández-Uribe, D., Holder, R. M., and Condit, C. B. (2022). Fluid-induced fault reactivation due to brucite + antigorite dehydration triggered the Mw7.1 September 19th Puebla-Morelos (Mexico) intermediate-depth earthquake. *Geophys. Res. Lett.*, 49, article no. e2022GL100814.

Hacker, B. R. (1997). Diagenesis and fault valve seismicity of crustal faults. *J. Geophys. Res.*, 102, 24459–24467.

Hadizadeh, J., Boyle, A. P., and Gaughan, A. E. (2024). A study of fluid overpressure microstructures from the creeping segment of the San Andreas fault. *J. Struct. Geol.*, 180, article no. 105065.

Hadizadeh, J., Mittempergher, S., Gratier, J. P., Renard, F., Di Toro, G., Richard, J., and Babaie, H. A. (2012). A microstructural study of fault rocks from the SAFOD: Implications for the deformation mechanisms and strength of the creeping segment of the San Andreas Fault. *J. Struct. Geol.*, 42, 246–260.

Hainzl, S. (2004). Seismicity patterns of earthquake swarms due to fluid intrusion and stress triggering. *Geophys. J. Int.*, 159, 1090–1096.

Hainzl, S. and Fischer, T. (2002). Indications for a successively triggered rupture growth underlying the 2000 earthquake swarm in Vogtland/NW Bohemia. *J. Geophys. Res.*, 107, article no. 2338.

Hancock, P. L. (1985). Brittle microtectonics: principle and practice. *J. Struct. Geol.*, 7, 437–457.

Handin, J. (1969). On the Coulomb-Mohr failure criterion. *J. Geophys. Res.*, 15, 5343–5348.

Hardebeck, J. L. and Michael, A. J. (2004). Stress orientations at intermediate angles to the San Andreas Fault, California. *J. Geophys. Res.*, 109, article no. B11303.

Healy, D. (2008). Damage patterns, stress rotations and pore fluid pressures in strike-slip fault zones. *J. Geophys. Res.*, 113, B12407.

Healy, J. D., Rubey, W. W., Griggs, D. T., and Raleigh, C. B. (1968). The Denver earthquakes. *Science*, 161, 1301–1310.

Henderson, I. H. C. and McCaig, A. M. (1996). Fluid pressure and salinity variations in shear-zone related veins, central Pyrenees, France: Implications for the fault-valve model. *Tectonophysics*, 262, 321–348.

Hirono, T., Fujimoto, K., Yokoyama, T., Hamada, Y., Tanikawa, W., Tadai, O., Mishima, T., Tanimizu, M., Lin, W., Soh, W., and Song, S. R. (2008). Clay mineral reactions caused by frictional heating during an earthquake: An example from the Taiwan Chelungpu fault. *Geophys. Res. Lett.*, 35, L16303.

Hirose, T., Hamada, Y., Tanikawa, W., et al. (2021). High fluid-pressure patches beneath the décollement: A potential source of slow earthquakes in the Nankai Trough off cape Muroto. *J. Geophys. Res.*, 126, article no. e2021JB021831.

Holdsworth, R. E., Van Diggelen, E. W. E., Spiers, C. J., De Bresser, J. H. P., Walker, R. J., and Bowen, L. (2011). Fault rocks from the SAFOD core samples: implications for weakening at shallow depths along the San Andreas Fault, California. *J. Struct. Geol.*, 33, 132–144.

Hoover, W. F., Penniston-Dorland, S., Baumgartner, L., Bouvier, A. S., Dragovic, B., Locatelli, M., Angiboust, S., and Agard, P. (2022). Episodic fluid flow in an eclogite-facies shear zone: Insights from Li isotope zoning in garnet. *Geology*, 50, 746–750.

Horton, S. (2012). Disposal of hydrofracking waste fluid by injection into subsurface aquifers triggers earthquake swarm in central Arkansas with potential for damaging earthquake. *Seismol. Res. Lett.*, 83, 250–260.

Housen, B. A., Tobin, H. J., Labaume, P., Leitch, E. C., and Maltman, A. J. (1996). Strain decoupling across the decollement of the Barbados accretionary prism. *Geology*, 24, 127–130.

Houston, H. (2015). Deep earthquakes. In Schubert, G., editor, *Treatise on Geophysics*, volume 4, pages 329–354. Elsevier, Oxford, 2nd edition.

Hubbert, M. K. and Rubey, W. W. (1959). Role of fluid pressure in mechanics of overthrust faulting I. Mechanics of fluid-filled porous solids and its application to overthrust faulting. *Geol. Soc. Am. Bull.*, 70, 115–166.

Hubbert, M. K. and Willis, D. G. (1957). Mechanics of hydraulic fracturing. *Trans. Am. Inst. Min. Eng.*, 210, 153–168.

Hürzeler, J. P. and Abart, R. (2008). Fluid flow and rock alteration along the Glarus Thrust. *Swiss J. Geosci.*, 101, 251–268.

Husen, S. and Kissling, E. (2001). Postseismic fluid flow after the large subduction earthquake of Antofagasta, Chile. *Geology*, 29, 847–850.

Hyndman, R. D., Wang, K., Yuan, T., and Spence, G. D. (1993). Tectonic sediment thickening, fluid expulsion, and the thermal regime of subduction zone accretionary prisms: The Cascadia margin off Vancouver Island. *J. Geophys. Res.*, 98, 21865–21876.

Janssen, C., Michel, G. W., Bau, M., Lüders, V., and Mühle, K. (1997). The North Anatolian Fault Zone and the role of fluids in seismogenic deformation. *J. Geol.*, 105, 387–404.

Jeanne, P., Guglielmi, Y., Rinaldi, A. P., and Rutqvist, J. (2014). The effects of lateral property variations on fault-zone reactivation by fluid pressurization: Application to CO_2 pressurization effects within major and undetected fault zones. *J. Struct. Geol.*, 62, 97–108.

Jefferies, S. P., Holdsworth, R. E., Wibberley, C. A. J., Shimamoto, T., and Spiers, C. J. (2006). The nature and importance of phyllonite development in crustal-scale fault cores; an example from the Median Tectonic Line, Japan. *J. Struct. Geol.*, 28, 220–235.

Jenatton, L., Guiguet, R., Thouvenot, F., and Daix, N. (2007). The 16,000-event 2003–2004 earthquake swarm in Ubaye (French Alps). *J. Geophys. Res.*, 112, B11304.

John, T. and Schenk, V. (2006). Interrelations between intermediate-depth earthquakes and fluid flow within subducting oceanic plates: Constraints from eclogite facies pseudotachylytes. *Geology*, 34, 557–560.

Jordan, P. (1992). Evidence for large-scale decoupling in the Triassic evaporites of Northern Switzerland: an overview. *Eclogae Geol. Helv.*, 85, 677–693.

Karabulut, H., Ozalaybey, S., Taymaz, T., Aktar, M., Selvi, O., and Kocaoglu, A. (2003). A tomographic image of the shallow crustal structure in the Eastern Marmara. *Geophys. Res. Lett.*, 30, article no. 2277.

Karaş, M., Tank, S. B., Ogawa, Y., Oshiman, N., Matsushima, M., and Honkura, Y. (2020). Probing the relationship between electrical conductivity and creep through upper crustal fluids along the western part of the North Anatolian Fault with three-dimensional magnetotellurics. *Tectonophysics*, 791, article no. 228561.

Katayama, I., Terada, T., Okazaki, K., and Tanikawa, W. (2012). Episodic tremor and slow slip potentially linked to permeability contrasts at the Moho. *Nat. Geosci.*, 5, 731–734.

Kato, A., Iidaka, T., Ikuta, R., Yoshida, Y., Katsumata, K., et al. (2010). Variations of fluid pressure within the subducting oceanic crust and slow earthquakes. *Geophys. Res. Lett.*, 37, article no. L14310.

Kato, A., Iidaka, T., Kurashimo, E., Nakagawa, S., Hirata, N., and Iwasaki, T. (2007). Delineation of probable asperities on the Atotsugawa fault, central Japan, using a dense temporary seismic network. *Geophys. Res. Lett.*, 34, article no. L09318.

Kerrich, R., Kamineni, D. C., Borre, D., Baldwin, D. K., McLarty, E., and Thivierge, R. H. (1987). Cyclic deformation and chemical transport in the Folson Lake fault zone, East Bull Lake anorthosite-gabbro complex: evidence for seismic pumping? *Appl. Geochem.*, 2, 103–126.

Kimura, G., Hina, S., Hamada, Y., Kameda, J., Tsuji, T., Kinoshita, M., and Yamaguchi, A. (2012). Runaway slip to the trench due to rupture of highly pressurized megathrust beneath the middle trench slope: the tsunamigenesis of the 2011 Tohoku earthquake off the east coast of northern Japan. *Earth Planet. Sci. Lett.*, 339, 32–45.

King, G. C. P., Stein, R. S., and Lin, J. (1994). Static stress changes and the triggering of earthquakes. *Bull. Seismol. Soc. Am.*, 84, 935–953.

Kitajima, H., Chester, F. M., and Chester, J. S. (2011). Dynamic weakening of gouge layers in high-speed shear experiments: Assessment of temperature-dependent friction, thermal pressurization, and flash heating. *J. Geophys. Res.*, 116, article no. B08309.

Kitajima, H. and Saffer, D. M. (2012). Elevated pore pressure and anomalously low stress in regions of low frequency earthquakes along the Nankai Trough subduction megathrust. *Geophys. Res. Lett.*, 39, article no. L23301.

Kodaira, S., Iidaka, T., Kato, A., Park, J. O., Iwasaki, T., and Kaneda, Y. (2004). High pore fluid pressure may cause silent slip in the Nankai Trough. *Science*, 304, 1295–1298.

Koerner, A., Kissling, E., and Miller, S. A. (2004). A model of deep crustal fluid flow following the Mw = 8.0 Antofagasta, Chile, earthquake. *J. Geophys. Res.*, 109, article no. B06307.

Kopf, A., Behrmann, J. H., Deyhle, A., Roller, S., and Erlenkeuser, H. (2003). Isotopic evidence (B, C, O) of deep fluid processes in fault rocks from the active Woodlark Basin detachment zone. *Earth Planet. Sci. Lett.*, 208, 51–68.

Kuge, K., Kase, Y., Urata, Y., Campos, J., and Perez, A. (2010). Rupture characteristics of the 2005 Tarapaca, northern Chile, intermediate-depth earthquake: Evidence for heterogeneous fluid distribution across the subducting oceanic plate? *J. Geophys. Res.*, 115, article no. B09305.

Lachenbruch, A. H. (1980). Frictional heating, fluid pressure, and the resistance to fault motion. *J. Geophys. Res.*, 85, 6097–6112.

Lacombe, O. and Mouthereau, F. (2002). Basement-involved shortening and deep detachment tectonics in forelands of orogens: Insights from recent collision belts (Taiwan, Western Alps, Pyrenees). *Tectonics*, 21(4), 12–1–12–22.

Lacroix, B., Leclère, H., Buatier, M., and Fabbri, O. (2013). Weakening processes in thrust faults: insights from the Monte Perdido thrust fault (southern Pyrenees, Spain). *Geofluids*, 13, 56–65.

Leclère, H. and Calais, E. (2019). A parametric analysis of fault reactivation in the New Madrid Seismic Zone: The role of pore fluid overpressure. *J. Geophys. Res.*, 124, 10630–10648.

Leclère, H., Daniel, G., Fabbri, O., Cappa, F., and Thouvenot, F. (2013). Tracking fluid pressure build-up from focal mechanisms during the 2003–2004 Ubaye seismic swarm, France. *J. Geophys. Res.*, 118, 4461–4476.

Leclère, H. and Fabbri, O. (2013). A new three-dimensional method of fault reactivation analysis. *J. Struct. Geol.*, 48, 153–161.

Leclère, H., Fabbri, O., Daniel, G., and Cappa, F. (2012). Reactivation of a strike-slip fault by fluid overpressuring in the southwestern French-Italian Alps. *Geophys. J. Int.*, 189, 29–37.

Lecomte, E., Le Pourhiet, L., Lacombe, O., and Jolivet, L. (2011). A continuum mechanics approach to quantify brittle strain on weak faults: Application to the extensional reactivation of shallow dipping discontinuities. *Geophys. J. Int.*, 184, 1–11.

Lin, A. (2019). Thermal pressurization and fluidization of pulverized cataclastic rocks formed in seismogenic fault zones. *J. Struct. Geol.*, 125, 278–284.

Lin, A., Yamashita, K., and Tanaka, M. (2013). Repeated seismic slips recorded in ultracataclastic veins along active faults of the Arima-Takatsuki Tectonic Line, southwestern Japan. *J. Struct. Geol.*, 48, 3–13.

Lindenfeld, M., Rümpker, G., Link, K., Koehn, D., and Batte, A. (2012). Fluid-triggered earthquake swarms in the Rwenzori region, East African Rift - Evidence for rift initiation. *Tectonophysics*, 566, 95–104.

Lombardi, A. M., Cocco, M., and Marzocchi, W. (2010). On the increase of background seismicity rate during the 1997–1998 Umbria-Marche, Central Italy, sequence: apparent variation or fluid-driven triggering? *Bull. Seismol. Soc. Am.*, 100, 1138–1152.

Lucente, F. P., De Gori, P., Margheriti, L., Piccinini, D., Di Bona, M., Chiarabba, C., and Agostinetti, N. P. (2010). Temporal variation of seismic velocity and anisotropy before the 2009 Mw 6.3 L'Aquila earthquake, Italy. *Geology*, 38, 1015–1018.

Magee, M. E. and Zoback, M. D. (1993). Evidence for a weak interplate thrust fault along the northern Japan subduction zone and implications for the mechanics of thrust faulting and fluid expulsion. *Geology*, 21, 809–812.

Malagnini, L., Lucente, F. P., De Gori, P., Akinci, A., and

Munafò, I. (2012). Control of pore fluid pressure diffusion on fault failure mode: Insights from the 2009 L'Aquila seismic sequence. *J. Geophys. Res.*, 117, article no. B05302.

Manatschal, G. (1999). Fluid- and reaction-assisted low-angle normal faulting: evidence from rift-related brittle fault rocks in the Alps (Err Nappe, eastern Switzerland). *J. Struct. Geol.*, 21, 777–793.

Mandal, P., Srinagesh, D., Vijayaraghavan, R., Suresh, G., Naresh, B., et al. (2022). Seismic velocity imaging of the Kumaon-Garhwal Himalaya, India. *Nat. Hazards*, 111, 2241–2260.

Mase, C. W. and Smith, L. (1987). Effects of frictional heating on the thermal, hydrologic, and mechanical response of a fault. *J. Geophys. Res.*, 92, 6249–6272.

Matsubara, M., Obara, K., and Kasahara, K. (2009). Three-dimensional P-and S-wave velocity structures beneath the Japan Islands obtained by high-density seismic stations by seismic tomography. *Tectonophysics*, 454, 86–103.

Matsuda, T., Omura, K., Ikeda, R., Arai, T., Kobayashi, K., Shimada, K., Tanaka, H., Tomita, T., and Hirano, S. (2004). Fracture-zone conditions on a recently active fault: insights from mineralogical and geochemical analyses of the Hirabayashi NIED drill core on the Nojima fault, southwest Japan, which ruptured in the 1995 Kobe earthquake. *Tectonophysics*, 378, 143–163.

McGarr, A., Bekins, B., Burkardt, N., Dewey, J., Earle, P., Ellsworth, W., Ge, S., Hickman, S., Holland, A., Majer, E., Rubinstein, J., and Sheehan, A. (2015). Coping with earthquakes induced by fluid injection. *Science*, 347, 830–831.

McGarr, A., Simpson, D., and Seeber, L. (2002). Case histories of induced and triggered seismicity. In *International Geophysics*, volume 81A, pages 647–661. Elsevier, Amsterdam.

Melchiorre, E. B., Criss, R. E., and Davisson, M. L. (1999). Relationship between seismicity and subsurface fluids, central Coast Ranges, California. *J. Geophys. Res.*, 104, 921–930.

Menant, A., Angiboust, S., Monié, P., Oncken, O., and Guigner, J. M. (2018). Brittle deformation during Alpine basal accretion and the origin of seismicity nests above the subduction interface. *Earth Planet. Sci. Lett.*, 487, 84–93.

Micklethwaite, S. (2008). Optimally oriented "fault-valve" thrusts: Evidence for aftershock-related fluid pressure pulses? *Geochem. Geophys. Geosyst.*, 9, article no. Q04012.

Mikada, H., Ienaga, M., Goto, T. N., and Kasaya, T. (2006). Current research status and meaning of fluid pressure monitoring at the Nankai Trough. *J. Geography (Chigaku Zasshi)*, 115, 367–382.

Miller, S. A. (2020). Aftershocks are fluid-driven and decay rates controlled by permeability dynamics. *Nat. Commun.*, 11, article no. 5787.

Miller, S. A., Collettini, C., Chiaraluce, L., Cocco, M., Barchi, M., and Kaus, B. J. (2004). Aftershocks driven by a high-pressure CO_2 source at depth. *Nature*, 427, 724–727.

Mishra, O. P. and Zhao, D. (2004). Seismic evidence for dehydration embrittlement of the subducting Pacific slab. *Geophys. Res. Lett.*, 31, article no. L09610.

Mittempergher, S., Di Toro, G., Gratier, J. P., Hadizadeh, J., Smith, S. A., and Spiess, R. (2011). Evidence of transient increases of fluid pressure in SAFOD phase III cores. *Geophys. Res. Lett.*, 38, article no. L03301.

Mittempergher, S., Pennacchioni, G., and Di Toro, G. (2009). The effects of fault orientation and fluid infiltration on fault rock assemblages at seismogenic depths. *J. Struct. Geol.*, 31, 1511–1524.

Moore, D. E. and Lockner, D. A. (2011). Frictional strengths of talc-serpentine and talc-quartz mixtures. *J. Geophys. Res.*, 116, article no. B01403.

Moore, D. E. and Rymer, M. J. (2007). Talc-bearing serpentinite and the creeping section of the San Andreas fault. *Nature*, 448, 795–797.

Moore, J. C., Klaus, A., Bangs, N. L., et al. (1998). Consolidation patterns during initiation and evolution of a plate-boundary decollement zone: Northern Barbados accretionary prism. *Geology*, 26, 811–814.

Moore, J. C., Moore, G. F., Cochrane, G. R., and Tobin, H. J. (1995a). Negative-polarity seismic reflections along faults of the Oregon accretionary prism: indicators of overpressuring. *J. Geophys. Res.*, 100, 12895–12906.

Moore, J. C., Moran, K., MacKay, M. E., and Tobin, H. (1995b). 22. Frontal thrust, Oregon accretionary prism: Geometry, physical properties, and fluid pressure. In *Proceedings of the Ocean Drilling Program, Scientific Results*, volume 146, pages 359–366. Ocean Drilling Program, College Station, TX.

Moore, J. C., Shipley, T. H., Goldberg, D., et al. (1995c).

Abnormal fluid pressures and fault-zone dilation in the Barbados accretionary prism: Evidence from logging while drilling. *Geology*, 23, 605–608.

Moore, J. C. and Tobin, H. (1997). 17. Estimated fluid pressures of the Barbados accretionary prism and adjacent sediments. In Shipley, T. H., Ogawa, Y., Blum, P., and Bahr, J. M., editors, *Proceedings of the Ocean Drilling Program, Scientific Results*, volume 156, pages 229–238. Ocean Drilling Program, College Station, TX.

Moore, J. C. and Vrolijk, P. (1992). Fluids in accretionary prisms. *Rev. Geophys.*, 30, 113–135.

Moreno, M., Haberland, C., Oncken, O., Rietbrock, A., Angiboust, S., and Heidbach, O. (2014). Locking of the Chile subduction zone controlled by fluid pressure before the 2010 earthquake. *Nat. Geosci.*, 7, 292–296.

Moretti, M., De Gori, P., and Chiarabba, C. (2009). Earthquake relocation and three-dimensional Vp and Vp/Vs models along the low angle Alto Tiberina fault (central Italy): Evidence for fluid overpressure. *Geophys. J. Int.*, 176, 833–846.

Morrow, C., Radney, B., and Byerlee, J. (1992). Frictional strength and the effective pressure law of montmorillonite and illite clays. In Evans, B. and Wong, T.-F., editors, *Fault Mechanisms and Transport Properties of Rocks*, pages 69–88. Elsevier, New York.

Morrow, C. A., Moore, D. E., and Lockner, D. A. (2017). Frictional strength of wet and dry montmorillonite. *J. Geophys. Res.*, 122, 3392–3409.

Mount, V. S. and Suppe, J. (1987). State of stress near the San Andreas fault: Implications for wrench tectonics. *Geology*, 15, 1143–1146.

Mourgues, R. and Cobbold, P. R. (2003). Thrust wedges and fluid overpressures: Sandbox modelling involving pore fluids. *J. Geophys. Res.*, 111, article no. B05404.

Mugnier, J. L., Huyghe, P., Chalaron, E., and Mascle, G. (1994). Recent movements along the Main Boundary Thrust of the Himalayas: normal faulting in an over-critical thrust wedge? *Tectonophysics*, 238, 199–215.

Mullis, J. (1988). Rapid subsidence and upthrusting in the Northern Apennines, deduced by fluid inclusion studies in quartz crystals from Porretta Terme. *Bulletin Suisse de Minéralogie et Pétrographie*, 68, 157–170.

Nadeau, R. M. and Guilhem, A. (2009). Clustering and periodic recurrence of microearthquakes on the San Andreas Fault at Parkfield, California. *Science*, 267, 503–507.

Nakajima, J., Hasegawa, A., and Kita, S. (2011). Seismic evidence for reactivation of a buried hydrated fault in the Pacific slab by the 2011 M9.0 Tohoku earthquake. *Geophys. Res. Lett.*, 38, article no. L00G06.

Nakajima, J., Matsuzawa, T., Hasegawa, A., and Zhao, D. (2001). Three-dimensional structure of V_p, V_s, and V_p/V_s beneath northeastern Japan: Implications for arc magmatism and fluids. *J. Geophys. Res.*, 106, 21843–21857.

Neuzil, C. E. (1995). Abnormal pressures as hydrodynamic phenomena. *Am. J. Sci.*, 295, 742–786.

Nguyen, P. T., Cox, S. F., Harris, L. B., and Powell, C. M. (1998). Fault-valve behaviour in optimally oriented shear zones: an example at the Revenge gold mine, Kambalda, Western Australia. *J. Struct. Geol.*, 20, 1625–1640.

Noda, H. and Shimamoto, T. (2003). Thermal pressurization and slip-weakening distance of a fault: An example of the Hanaore Faut, Southwest Japan. *Bull. Seismol. Soc. Am.*, 95, 1224–1233.

Noir, J., Jacques, E., Békri, S., Adler, P. M., Tapponnier, P., and King, G. C. P. (1997). Fluid flow triggered migration of events in the 1989 Dobi earthquake sequence of Central Afar. *Geophys. Res. Lett.*, 24, 2335–2338.

Nostro, C., Chiaraluce, L., Cocco, M., Baumont, D., and Scotti, O. (2005). Coulomb stress changes caused by repeated normal faulting earthquakes during the 1997 Umbria-Marche (central Italy) seismic sequence. *J. Geophys. Res.*, 110, article no. B05S20.

Nur, A. (1974). Matsuhiro, Japan, earthquake swarm: confirmation of the dilatancy-fluid diffusion model. *Geology*, 2, 217–221.

Nur, A. and Booker, J. R. (1972). Aftershocks caused by pore fluid flow? *Science*, 175, 885–887.

Obara, K. (2002). Nonvolcanic deep tremor associated with subduction in Southwest Japan. *Science*, 296, 1679–1681.

Park, J. O., Fujie, G., Wijerathne, L., Hori, T., Kodaira, S., Fukao, Y., Moore, G. F., Bangs, N., Kuramoto, S., and Taira, A. (2010). A low-velocity zone with weak reflectivity along the Nankai subduction zone. *Geology*, 38, 283–286.

Park, J. O., Tsuru, T., Kodaira, S., Cummins, P. R., and

Kaneda, Y. (2002). Splay fault branching along the Nankai subduction zone. *Science*, 297, 1157–1160.

Park, J. O., Tsuru, T., Kodaira, S., Nakanishi, A., Miura, S., Kaneda, Y., Kono, Y., and Takahashi, N. (2000). Outofsequence thrust faults developed in the coseismic slip zone of the 1946 Nankai earthquake (Mw = 8.2) off Shikoku, southwest Japan. *Geophys. Res. Lett.*, 27, 1033–1036.

Parotidis, M., Rothert, E., and Shapiro, S. A. (2003). Pore-pressure diffusion: A possible triggering mechanism for the earthquake swarms 2000 in Vogtland/NW-Bohemia, central Europe. *Geophys. Res. Lett.*, 30, article no. 2075.

Passelègue, F., Fabbri, O., Dubois, M., and Ventalon, S. (2014). Evidence for fluid overpressuring along an Oligocene out-of-sequence thrust in the Shimanto accretionary prism, SW Japan. *J. Asia Earth Sci.*, 86, 12–24.

Paulatto, M., Laigle, M., Galve, A., Charvis, P., Sapin, M., Bayrakci, G., Evain, M., and Kopp, H. (2017). Dehydration of subducting slow-spread oceanic lithosphere in the Lesser Antilles. *Nat. Commun.*, 8, article no. 15980.

Peacock, S. M. (2009). Thermal and metamorphic environment of subduction zone episodic tremor and slip. *J. Geophys. Res.*, 114, article no. B00A07.

Peacock, S. M., Christensen, N. I., Bostock, M. G., and Audet, P. (2011). High pore pressures and porosity at 35 km depth in the Cascadia subduction zone. *Geology*, 39, 471–474.

Pezzo, G., De Gori, P., Lucente, F. P., and Chiarabba, C. (2018). Pore pressure pulse drove the 2012 Emilia (Italy) series of earthquakes. *Geophys. Res. Lett.*, 45, 682–690.

Pfister, M., Greber, E., Schindler, C., Straub, C., Kahle, H. G., and Rybach, L. (2000). Geodynamics of the Marmara Sea region. Recent tectonic activity and the role of fluids at the western end of the North Anatolian Fault Zone. *Bulletin für Angewandte Geologie*, 5, 155–176.

Picazo, S., Cannat, M., Delacour, A., Escartín, J., Rouméjon, S., and Silantyev, S. (2012). Deformation associated with the denudation of mantle-derived rocks at the Mid-Atlantic Ridge 13°–15° N: The role of magmatic injections and hydrothermal alteration. *Geochem. Geophys. Geosyst.*, 13, article no. Q04G09.

Picazo, S., Manatschal, G., Cannat, M., and Andréani, M. (2013). Deformation associated to exhumation of serpentinized mantle rocks in a fossil Ocean Continent Transition: The Totalp unit in SE Switzerland. *Lithos*, 175, 255–271.

Plateaux, R., Bergerat, F., Béthoux, N., Villemin, T., and Gerbault, M. (2012). Implications of fracturing mechanisms and fluid pressure on earthquakes and fault slip data in the east Iceland rift zone. *Tectonophysics*, 581, 19–34.

Powley, D. E. (1990). Pressures and hydrogeology in petroleum basins. *Earth Sci. Rev.*, 29, 215–226.

Prejean, S., Stork, A., Ellsworth, W., Hill, D., and Julian, B. (2003). High precision earthquake locations reveal seismogenic structure beneath Mammoth Mountain, California. *Geophys. Res. Lett.*, 30, article no. 2247.

Provost, A. S. and Houston, H. (2001). Orientation of the stress field surrounding the creeping section of the San Andreas Fault: Evidence for a narrow mechanically weak fault zone. *J. Geophys. Res.*, 106, 11373–11386.

Pwavodi, J. and Doan, M. L. (2024). Direct assessment of the hydraulic structure of the plate boundary at the toe of the Nankai accretionary prism. *Geophys. J. Int.*, 236, 1125–1138.

Quattrocchi, F. (1999). In search of evidence of deep fluid discharges and pore pressure evolution in the crust to explain the seismicity style of the Umbria-Marche 1997–1998 seismic sequence (Central Italy). *Annali di Geofisica*, 42, 606–636.

Raimbourg, H., Famin, V., Canizares, A., and Le Trong, E. (2022). Fluid pressure changes recorded by trace elements in quartz. *Geochem. Geophys. Geosyst.*, 23, article no. e2022GC010346.

Raimbourg, H., Rajic, K., Famin, V., Moris-Muttoni, B., Palazzin, G., Fisher, D. M., Morell, K., Erdmann, S., Di Carlo, I., and Montmartin, C. (2021). Quartz vein geochemistry records deformation processes in convergent zones. *Geochem. Geophys. Geosyst.*, 22, article no. e2020GC009201.

Raimbourg, H., Vacelet, M., Ramboz, C., Famin, V., Augier, R., Palazzin, G., Yamaguchi, A., and Kimura, G. (2015). Fluid circulation in the depths of accretionary prisms: an example of the Shimanto Belt, Kyushu, Japan. *Tectonophysics*, 655, 161–176.

Raleigh, C. B., Healy, J. H., and Bredehoeft, J. D. (1976). An experiment in earthquake control at Rangely, Colorado. *Science*, 191, 1230–1237.

Ramsay, J. G. (1980). The crack-seal mechanism of rock deformation. *Nature*, 284, 135–139.

Rastogi, B. K., Chadha, R. K., Sarma, C. S. P., Mandal, P., Satyanarayana, H. V. S., Raju Narendra Kumar, I. P., Satyamurthy, C., and Rao, A. N. (1997). Seismicity at Warna reservoir (near Koyna) through 1995. *Bull. Seismol. Soc. Am.*, 87, 1484–1494.

Reynolds, S. J. and Lister, G. S. (1987). Structural aspects of fluid-rock interactions in detachment zones. *Geology*, 15, 362–366.

Rice, J. R. (1992). Fault stress states, pore pressure distributions, and the weakness of the San Andreas fault. *Int. Geophys.*, 51, 475–503.

Robert, F., Boullier, A. M., and Firdaous, K. (1995). Gold-quartz veins in metamorphic terranes and their bearing on the role of fluids in faulting. *J. Geophys. Res.*, 100, 12861–12879.

Roller, S., Behrmann, J. H., and Kopf, A. (2001). Deformation fabrics of faulted rocks, and some syntectonic stress estimates from the active Woodlark Basin detachment zone. *Geol. Soc. London Spec. Publ.*, 187, 319–334.

Rowe, C. D., Meneghini, F., and Moore, J. C. (2009). Fluid-rich damage zone of an ancient out-of-sequence thrust, Kodiak Islands, Alaska. *Tectonics*, 28, article no. TC1006.

Saffer, D. M., Silver, E. A., Fisher, A. T., Tobin, H., and Moran, K. (2000). Inferred pore pressures at the Costa Rica subduction zone: Implications for dewatering processes. *Earth Planet. Sci. Lett.*, 177, 193–207.

Saffer, D. M. and Tobin, H. J. (2011). Hydrogeology and mechanics of subduction zone forearcs: Fluid flow and pore pressure. *Annu. Rev. Earth Planet. Sci.*, 39, 157–186.

Saffer, D. M. and Wallace, L. M. (2015). The frictional, hydrologic, metamorphic and thermal habitat of shallow slow earthquakes. *Nat. Geosci.*, 8, 594–600.

Schleicher, A. M., Tourscher, S. N., van der Pluijm, B. A., and Warr, L. N. (2009a). Constraints on mineralization, fluidrock interaction, and mass transfer during faulting at 2–3 km depth from the SAFOD drill hole. *J. Geophys. Res.*, 114, article no. B04202.

Schleicher, A. M., Warr, L. N., and Van Der Pluijm, B. A. (2009b). On the origin of mixed-layered clay minerals from the San Andreas Fault at 2.5–3 km vertical depth (SAFOD drillhole at Parkfield, California). *Contrib. Mineral. Petrol.*, 157, 173–187.

Schmidt, W. L. and Platt, J. P. (2022). Stress, microstructure, and deformation mechanisms during subduction underplating at the depth of tremor and slow slip, Franciscan Complex, northern California. *J. Struct. Geol.*, 154, article no. 104469.

Screaton, E. J. and Saffer, D. M. (2005). Fluid expulsion and overpressure development during initial subduction at the Costa Rica convergent margin. *Earth Planet. Sci. Lett.*, 233, 361–374.

Secor, D. T. (1965). Role of fluid pressure in jointing. *Am. J. Sci.*, 263, 633–646.

Segall, P. and Rice, J. R. (2006). Does shear heating of pore fluid contribute to earthquake nucleation? *J. Geophys. Res.*, 111, article no. B09316.

Selverstone, J., Axen, G. J., and Bartley, J. M. (1995). Fluid inclusion constraints on the kinematics of footwall uplift beneath the Brenner Line normal fault, eastern Alps. *Tectonics*, 14, 264–278.

Selverstone, J., Axen, G. J., and Luther, A. (2012). Fault localization controlled by fluid infiltration into mylonites: Formation and strength of lowangle normal faults in the midcrustal brittleplastic transition. *J. Geophys. Res.*, 117, article no. B06210.

Seno, T. (2009). Determination of the pore fluid pressure ratio at seismogenic megathrusts in subduction zones: Implications for strength of asperities and Andeantype mountain building. *J. Geophys. Res.*, 114, article no. B05405.

Seno, T. and Yamasaki, T. (2003). Low-frequency tremors, intraslab and interplate earthquakes in Southwest Japan—from a viewpoint of slab dehydration. *Geophys. Res. Lett.*, 30, article no. 2171.

Shaddox, H. R. and Schwartz, S. Y. (2019). Subducted seamount diverts shallow slow slip to the forearc of the northern Hikurangi subduction zone, New Zealand. *Geology*, 47, 415–418.

Shelly, D. R., Beroza, G. C., Ide, S., and Nakamura, S. (2006a). Low-frequency earthquakes in Shikoku, Japan, and their relationship to episodic tremor and slip. *Nature*, 442, 188–191.

Shelly, D. R., Beroza, G. C., Zhang, H., Thurber, C. H., and Ide, S. (2006b). High-resolution subduction zone seismicity and velocity structure beneath Ibaraki Prefecture, Japan. *J. Geophys. Res.*, 111, article no. B06311.

Shelly, D. R., Ellsworth, W. L., and Hill, D. P. (2016). Fluid-faulting evolution in high definition: Connecting fault structure and frequency-magnitude variations during the 2014 Long Valley Caldera, California, earthquake swarm. *J. Geophys. Res.*, 121, 1776–1795.

Sherkati, S., Letouzey, J., and Frizon de Lamotte, D. (2006). Central Zagros fold-thrust belt (Iran): New insights from seismic data, field observation, and sandbox modelling. *Tectonics*, 25, article no. TC4007.

Shiina, T., Nakajima, J., and Matsuzawa, T. (2013). Seismic evidence for high pore pressures in the oceanic crust: Implications for fluidrelated embrittlement. *Geophys. Res. Lett.*, 40, 2006–2010.

Shiina, T., Nakajima, J., Matsuzawa, T., Toyokuni, G., and Kita, S. (2017). Depth variations in seismic velocity in the subducting crust: Evidence for fluid-related embrittlement for intermediate-depth earthquakes. *Geophys. Res. Lett.*, 44, 810–817.

Shipley, T. H., Moore, G. F., Bangs, N. L., Moore, J. C., and Stoffa, P. L. (1994). Seismically inferred dilatancy distribution, northern Barbados Ridge decollement: Implications for fluid migration and fault strength. *Geology*, 22, 411–414.

Sibson, R. H. (1973). Interactions between temperature and pore-pressure during earthquake faulting: A mechanism for spatial or total stress relief. *Nat. Phys. Sci.*, 243, 66–68.

Sibson, R. H. (1985). A note on fault reactivation. *J. Struct. Geol.*, 7, 751–754.

Sibson, R. H. (1989). High-angle reverse faulting in northern New Brunswick, Canada, and its implications for fluid pressure levels. *J. Struct. Geol.*, 11, 873–877.

Sibson, R. H. (1990). Conditions for fault-valve behavior. *Geol. Soc. London Spec. Publ.*, 54, 15–28.

Sibson, R. H. (2007). An episode of fault-valve behaviour during compressional inversion?—The 2004 Mj 6.8 Mid-Niigata Prefecture, Japan, earthquake sequence. *Earth Planet. Sci. Lett.*, 257, 188–199.

Sibson, R. H. (2009). Rupturing in overpressured crust during compressional inversion—the case from NE Honshu, Japan. *Tectonophysics*, 473, 404–416.

Sibson, R. H. (2013). Stress switching in subduction forearcs: implications for overpressure containment and strength cycling on megathrusts. *Tectonophysics*, 600, 142–152.

Sibson, R. H., Moore, J. M. M., and Rankin, A. H. (1975). Seismic pumping—a hydrothermal fluid transport mechanism. *J. Geol. Soc.*, 131, 653–659.

Sibson, R. H., Robert, F., and Poulsen, K. H. (1988). High-angle reverse faults, fluid-pressure cycling, and mesothermal gold-quartz deposits. *Geology*, 16, 551–555.

Sibson, R. H. and Rowland, J. V. (2003). Stress, fluid pressure and structural permeability in seismogenic crust, North Island, New Zealand. *Geophys. J. Int.*, 154, 584–594.

Sibson, R. H. and Scott, J. (1998). Stress/fault controls on the containment and release of overpressured fluids: examples from gold-quartz vein systems in Juneau, Alaska; Victoria, Australia and Otago, New Zealand. *Ore Geol. Rev.*, 13, 293–306.

Skarbek, R. M. and Saffer, D. M. (2009). Pore pressure development beneath the décollement at the Nankai subduction zone: Implications for plate boundary fault strength and sediment dewatering. *J. Geophys. Res.*, 114, article no. B07401.

Sleep, N. H. and Blanpied, M. L. (1992). Creep, compaction and the weak rheology of major faults. *Nature*, 359, 687–692.

Smith, B. M., Reynolds, S. J., Day, H. W., and Bodnar, R. J. (1991). Deep-seated fluid involvement in ductile-brittle deformation and mineralization, South Mountains metamorphic core complex, Arizona. *Geol. Soc. Am. Bull.*, 103, 559–569.

Sommaruga, A., Mosar, J., Schori, M., and Gruber, M. (2017). The role of the Triassic evaporites underneath the North Alpine Foreland. In *Permo-Triassic Salt Provinces of Europe, North Africa and the Atlantic Margins*, pages 447–466. Elsevier, Amsterdam.

Song, T. R. A., Helmberger, D. V., Brudzinski, M. R., Clayton, R. W., Davis, P., Pérez-Campos, X., and Singh, S. K. (2009). Subducting slab ultra-slow velocity layer coincident with silent earthquakes in southern Mexico. *Science*, 324, 502–506.

Spandler, C., Pettke, T., and Rubatto, D. (2011). Internal and external fluid sources for eclogite-facies veins in the Monviso meta-ophiolite, Western Alps: implications for fluid flow in subduction zones. *J. Petrol.*, 52, 1207–1236.

Sugioka, H., Okamoto, T., Nakamura, T., Ishihara, Y., Ito, A., Obana, K., Kinoshita, M., Nakahigashi, K., Shinohara, M., and Fukao, Y. (2012). Tsunamigenic potential of the shallow subduction plate boundary inferred from slow seismic slip. *Nat. Geosci.*, 5, 414–418.

Suppe, J. and Wittke, J. H. (1977). Abnormal pore-fluid pressures in relation to stratigraphy and structure in the active fold-and-thrust belt of northwestern Taiwan. *Pet. Geol. Taiwan*, 14, 11–24.

Sutherland, R., Townend, J., Toy, V., et al. (2017). Extreme hydrothermal conditions at an active plate-bounding fault. *Nature*, 546, 137–141.

Sutherland, R., Toy, V. G., Townend, J., et al. (2012). Drilling reveals fluid control on architecture and rupture of the Alpine fault, New Zealand. *Geology*, 40, 1143–1146.

Tank, S. B., Honkura, Y., Ogawa, Y., Matsushima, M., Oshiman, N., Tunçer, M. K., Çelik, C., Tolak, E., and Işıkara, A. M. (2005). Magnetotelluric imaging of the fault rupture area of the 1999 Izmit (Turkey) earthquake. *Phys. Earth Planet. Inter.*, 150, 213–225.

Tarling, M. S., Smith, S. A., and Scott, J. M. (2019). Fluid overpressure from chemical reactions in serpentinite within the source region of deep episodic tremor. *Nat. Geosci.*, 12, 1034–1042.

Tauzin, B., Reynard, B., Perrillat, J., Debayle, E., and Bodin, T. (2017). Deep crustal fracture zones control fluid escape and the seismic cycle in the Cascadia subduction zone. *Earth Planet. Sci. Lett.*, 460, 1–11.

Terakawa, T., Miller, S. A., and Deichmann, N. (2012). High fluid pressure and triggered earthquakes in the enhanced geothermal system in Basel, Switzerland. *J. Geophys. Res.*, 117, article no. B07305.

Terakawa, T., Zoporowski, A., Galvan, B., and Miller, S. A. (2010). High-pressure fluid at hypocentral depths in the L'Aquila region inferred from earthquake focal mechanisms. *Geology*, 38, 995–998.

Thomas, A. M., Nadeau, R. M., and Bürgmann, R. (2009). Tremor-tide correlations and near-lithostatic pore pressure on the deep San Andreas fault. *Nature*, 462, 1048–1051.

Tobin, H. J., Moore, J. C., and Moore, G. F. (1994). Fluid pressure in the frontal thrust of the Oregon accretionary prism: Experimental constraints. *Geology*, 22, 979–982.

Tobin, H. J. and Saffer, D. M. (2009). Elevated fluid pressure and extreme mechanical weakness of a plate boundary thrust, Nankai Trough subduction zone. *Geology*, 37, 679–682.

Tsuji, T., Tokuyama, H., Costa-Pisani, P., and Moore, G. (2008). Effective stress and pore pressure in the Nankai accretionary prism off the Muroto Peninsula, southwestern Japan. *J. Geophys. Res.*, 113, article no. B11401.

Ujiie, K., Hisamitsu, T., and Taira, A. (2003). Deformation and fluid pressure variation during initiation and evolution of the plate boundary décollement zone in the Nankai accretionary prism. *J. Geophys. Res.*, 108, article no. 2398.

Ujiie, K., Kameyama, M., and Yamaguchi, A. (2010). Geological record of thermal pressurization and earthquake instability of subduction thrusts. *Tectonophysics*, 485, 260–268.

Ujiie, K., Saishu, H., Fagereng, Å., Nishiyama, N., Otsubo, M., Masuyama, H., and Kagi, H. (2018). An explanation of episodic tremor and slow slip constrained by crack-seal veins and viscous shear in subduction mélange. *Geophys. Res. Lett.*, 45, 5371–5379.

Ujiie, K., Tsutsumi, A., and Kameda, J. (2011). Reproduction of thermal pressurization and fluidization of clay-rich fault gouges by high-velocity friction experiments and implications for seismic slip in natural faults. *Geol. Soc. London Spec. Publ.*, 359, 267–285.

Ujiie, K., Yamaguchi, A., Kimura, G., and Toh, S. (2007). Fluidization of granular material in a subduction thrust at seismogenic depths. *Earth Planet. Sci. Lett.*, 259, 307–318.

Unruh, J. R., Davisson, M. L., Criss, R. E., and Moores, E. M. (1992). Implications of perennial saline springs for abnormally high fluid pressures and active thrusting in western California. *Geology*, 20, 431–434.

Van Wees, J. D., Buijze, L., Van Thienen-Visser, K., Nepveu, M., Wassing, B. B. T., Orlic, B., and Fokker, P. A. (2014). Geomechanics response and induced seismicity during gas field depletion in the Netherlands. *Geothermics*, 52, 206–219.

Vannucchi, P. and Leoni, L. (2007). Structural characterization of the Costa Rica décollement: Evidence for seismically-induced fluid pulsing. *Earth Planet. Sci. Lett.*, 262, 413–428.

Vannucchi, P., Remitti, F., Bettelli, G., Boschi, C., and Dallai, L. (2010). Fluid history related to the early Eocenemiddle Miocene convergent system of the Northern Apennines (Italy): Constraints from structural and isotopic studies. *J. Geophys. Res.*, 115, article no. B05405.

Vavryčuk, V. (2002). Non-double-couple earthquakes of 1997 January in West Bohemia, Czech Republic: evidence of tensile faulting. *Geophys. J. Int.*, 149, 364–373.

Vendeville, B. C. and Jackson, M. P. A. (1992a). The fall of diapirs during thin-skinned extension. *Mar. Pet. Geol.*, 9, 354–371.

Vendeville, B. C. and Jackson, M. P. A. (1992b). The rise of diapirs during thin-skinned extension. *Mar. Pet. Geol.*, 9, 331–354.

Vendeville, B. C., Pengcheng, T., Graveleau, F., Shaoying, H., and Wang, X. (2017). How the presence of a salt décollement in the sedimentary cover influences the behavior of subsalt thrusts in fold-and-thrust belts. *BSGF-Earth Sci. Bull.*, 188, article no. 37.

Vidale, J. E. and Shearer, P. M. (2006). A survey of 71 earthquake bursts across southern California: Exploring the role of pore fluid pressure fluctuations and aseismic slip as drivers. *J. Geophys. Res.*, 111, article no. B05312.

Viesca, R. C. and Garagash, D. I. (2015). Ubiquitous weakening of faults due to thermal pressurization. *Nat. Geosci.*, 8, 875–879.

Viete, D. R., Hacker, B. R., Allen, M. B., Seward, G. G. E., Tobin, M. J., Kelley, C. S., Cinque, G., and Duckworth, A. R. (2018). Metamorphic records of multiple seismic cycles during subduction. *Sci. Adv.*, 4, article no. eaaq0234.

Von Huene, R. (1985). Direct measurement of pore fluid pressure, Leg 84, Guatemala and Costa Rica. In *Initial Reports, Deep Sea Drilling Project leg 84*, pages 767–772. U.S. Government Publishing Office, Washington, DC.

Vrolijk, P. (1987). Tectonically driven fluid flow in the Kodiak accretionary complex, Alaska. *Geology*, 15, 466–469.

Vrolijk, P., Myers, G., and Moore, J. C. (1988). Warm fluid migration along tectonic melanges in the Kodiak Accretionary Complex, Alaska. *J. Geophys. Res.*, 93, 10313–10324.

Walder, J. and Nur, A. (1984). Porosity reduction and crustal pore pressure development. *J. Geophys. Res.*, 89, 11539–11548.

Waldhauser, F., Schaff, D. P., Diehl, T., and Engdahl, R. E. (2012). Splay faults imaged by fluid-driven aftershocks of the 2004 Mw 9.2 Sumatra-Andaman earthquake. *Geology*, 40, 243–246.

Wallace, L. M. (2020). Slow slip events in New Zealand. *Annu. Rev. Earth Planet. Sci.*, 48, 175–203.

Wallace, L. M. and Eberhart-Phillips, D. (2013). Newly observed, deep slow slip events at the central Hikurangi margin, New Zealand: Implications for downdip variability of slow slip and tremor, and relationship to seismic structure. *Geophys. Res. Lett.*, 40, 5393–5398.

Wang, X., Hu, W., Qiu, Y., Liu, Y., Jia, D., Cao, J., Liu, X., and Li, Y. (2022). Fluid inclusion evidence for extreme overpressure induced by gas generation in sedimentary basins. *Geology*, 50, 765–770.

Warren-Smith, E., Fry, B., Wallace, L., Chon, E., Henrys, S., Sheehan, A., Mochizuki, K., Schwartz, S., Webb, S., and Lebedev, S. (2019). Episodic stress and fluid pressure cycling in subducting oceanic crust during slow slip. *Nat. Geosci.*, 12, 475–481.

Wei, S., Avouac, J. P., Hudnut, K. W., Donnellan, A., Parker, J. W., Graves, R. W., Helmberger, D., Fielding, E., Liu, Z., Cappa, F., and Eneva, M. (2015). The 2012 Brawley swarm triggered by injection-induced aseismic slip. *Earth Planet. Sci. Lett.*, 422, 115–125.

Weijermars, R., Jackson, M. T., and Vendeville, B. (1993). Rheological and tectonic modeling of salt provinces. *Tectonophysics*, 217, 143–174.

Westaway, R. (1999). The mechanical feasibility of low-angle normal faulting. *Tectonophysics*, 308, 407–443.

White, S. H. and Knipe, R. J. (1978). Microstructure and cleavage development in selected slates. *Contrib. Mineral. Petrol.*, 66, 165–174.

Wibberley, C. A. and Shimamoto, T. (2005). Earthquake slip weakening and asperities explained by thermal pressurization. *Nature*, 436, 689–692.

Wintsch, R. P., Christoffersen, R., and Kronenberg, A. K. (1995). Fluid-rock reaction weakening of fault zones. *J. Geophys. Res.*, 100, 13021–13032.

Wiprut, D. and Zoback, M. D. (2000). Fault reactivation and fluid flow along a previously dormant normal fault in the northern North Sea. *Geology*, 28, 595–598.

Wood, J. R. and Boles, J. R. (1991). Evidence for episodic cementation and diagenetic recording of seismic pumping events, North Coles Levee, California, USA. *Appl. Geochem.*, 6, 509–521.

Yarce, J., Sheehan, A., Roecker, S., and Mochizuki, K. (2021). Seismic velocity heterogeneity of the Hikurangi subduction margin, New Zealand: Elevated pore pressures in a region with repeating slow slip events. *J. Geophys. Res.*, 126, article no. e2020JB021605.

Yeck, W. L., Weingarten, M., Benz, H. M., McNamara, D. E., Bergman, E. A., Herrmann, R. B., Rubinstein, J., and Earle, P. S. (2016). Farfield pressurization likely caused one of the largest injection induced earthquakes by reactivating a large preexisting basement fault structure. *Geophys. Res. Lett.*, 43, 10–198.

Yerkes, R. F., Levine, P., and Wentworth, C. M. (1985). Abnormally high fluid pressures in the region of the Coalinga earthquakes—a preliminary report. *US Geological Survey Open-File Report*, 85, 344–375.

Yin, A. (1989). Origin of regional, rooted lowangle normal faults: A mechanical model and its tectonic implications. *Tectonics*, 8, 469–482.

Yoshida, K., Hasegawa, A., and Yoshida, T. (2016). Temporal variation of frictional strength in an earthquake swarm in NE Japan caused by fluid migration. *J. Geophys. Res.*, 121, 5953–5965.

Yoshida, K., Uchida, N., Matsumoto, Y., et al. (2023). Updip fluid flow in the crust of the northeastern Noto Peninsula, Japan, triggered the 2023 Mw 6.2 Suzu earthquake during swarm activity. *Geophys. Res. Lett.*, 50, article no. e2023GL106023.

Yuan, X. P., Christie-Blick, N., and Braun, J. (2018). Mechanical properties of the Sevier Desert detachment: An application of critical Coulomb wedge theory. *Geophys. Res. Lett.*, 45, 7417–7424.

Yuan, X. P., Olive, J. A., and Braun, J. (2020). Partially locked lowangle normal faults in cohesive upper crust. *Tectonics*, 39, article no. e2019TC005753.

Yukutake, Y., Ito, H., Honda, R., Harada, M., Tanada, T., and Yoshida, A. (2011). Fluid-induced swarm earthquake sequence revealed by precisely determined hypocenters and focal mechanisms in the 2009 activity at Hakone volcano, Japan. *J. Geophys. Res.*, 116, article no. B04308.

Zencher, F., Bonafede, M., and Stefansson, R. (2006). Near-lithostatic pore pressure at seismogenic depths: a thermoporoelastic model. *Geophys. J. Int.*, 166, 1318–1334.

Zhang, L., Lei, X., Liao, W., Li, J., and Yao, Y. (2019). Statistical parameters of seismicity induced by the impoundment of the Three Gorges Reservoir, Central China. *Tectonophysics*, 751, 13–22.

Zhao, D., Kanamori, H., Negishi, H., and Wiens, D. (1996). Tomography of the source area of the 1995 Kobe earthquake: evidence for fluids at the hypocenter? *Science*, 274, 1891–1894.

Zoback, M. D. and Gorelick, S. M. (2012). Earthquake triggering and large-scale geologic storage of carbon dioxide. *Proc. Natl Acad. Sci.*, 109, 10164–10168.

Zoback, M. D. and Harjes, H. P. (1997). Injection-induced earthquakes and crustal stress at 9 km depth at the KTB deep drilling site, Germany. *J. Geophys. Res.*, 102, 18477–18491.

Zoback, M. D., Zoback, M. L., Mount, V. S., Suppe, J., Eaton, J. P., Healy, J. H., Oppenheimer, D., Reasenberg, P., Jones, L., Raleigh, C. B., Wong, I. G., Scotti, O., and Wentworth, C. (1987). New evidence on the state of stress of the San Andreas fault system. *Science*, 238, 1105–1111.